

1 **AIMERG: a new Asian precipitation dataset (0.1°/half-hourly, 2000-2015) by calibrating GPM**
2 **IMERG at daily scale using APHRODITE**

3 Ziqiang Ma¹, Jintao Xu², Siyu Zhu¹, Jun Yang³, Guoqiang Tang^{4,5}, Yuanjian Yang⁶, Zhou Shi², Yang
4 Hong^{1,7}

5 ¹*Institute of Remote Sensing and Geographical Information Systems, School of Earth and Space Sciences, Peking*
6 *University, Beijing, 100871, China*

7 ²*Institute of Agricultural Remote Sensing and Information Technology Application, College of Environmental and*
8 *Resource Sciences, Zhejiang University, Hangzhou, 310058, China*

9 ³*National Satellite Meteorological Centre, China Meteorological Administration, Beijing, 100081, China*

10 ⁴*University of Saskatchewan Coldwater Lab, Canmore, Alberta, Canada, T1W 3G1*

11 ⁵*Centre for Hydrology, University of Saskatchewan, Saskatoon, Saskatchewan, Canada, S7N 1K2*

12 ⁶*School of Atmospheric Physics, Nanjing University of Information Science and Technology, Nanjing 210044, China*

13 ⁷*School of Civil Engineering and Environmental Science, University of Oklahoma, Norman, OK, 73019, United States*

14 Correspondences: Ziqiang Ma (ziqma@pku.edu.cn); Prof. Yang Hong (yanghong@ou.edu)

15

16 **AIMERG: a new Asian precipitation dataset (0.1°/half-hourly, 2000-2015) by calibrating GPM**
17 **IMERG at daily scale using APHRODITE**

18

19 **Highlights**

20 ● **A new effective daily calibration approach, DSTDCA, for improving GPM IMERG**

21 ● **A new AIMERG precipitation data (0.1°/half-hourly, 2000-2015, Asia) is provided**

22 ● **Bias of AIMERG is significantly improved compared with that of IMERG**

23 ● **APHRODITE is more suitable than GPCC in anchoring IMERG over the Asia**

24

25

26

27

28

29

30

31 **Abstract**

32 Precipitation estimates with fine quality and spatio-temporal resolutions play significant roles in
33 understanding the global and regional cycles of water, carbon and energy. Satellite-based precipitation
34 products are capable of detecting spatial patterns and temporal variations of precipitation at fine
35 resolutions, which is particularly useful over poorly gauged regions. However, satellite-based
36 precipitation products are the indirect estimates of precipitation, inherently containing regional and
37 seasonal systematic biases and random errors. In this study, focusing on the potential drawbacks in
38 generating Integrated Multi-satellitE Retrievals for Global Precipitation Measurement (IMERG) and its
39 recently updated retrospective IMERG in the Tropical Rainfall Measuring Mission (TRMM) era (finished
40 in July, 2019), which were only calibrated at monthly scale using ground observations, Global
41 Precipitation Climatology Centre (GPCC, 1.0°/Monthly), we aim to propose a new calibration algorithm
42 for IMERG at daily scale, and to provide a new AIMERG precipitation dataset (0.1°/ half-hourly, 2000-
43 2015, Asia) with better quality, calibrated by Asian Precipitation Highly Resolved Observational Data
44 Integration (APHRODITE, 0.25°/Daily) at the daily scale for the Asian applications. And the main
45 conclusions include but not limited to: (1) the proposed daily calibration algorithm (Daily Spatio-
46 Temporal Disaggregation Calibration Algorithm, DSTDCA) is effective in considering the advantages
47 from both satellite-based precipitation estimates and the ground observations; (2) AIMERG performs
48 better than IMERG at different spatio-temporal scales, in terms of both systematic biases and random
49 errors, over the China Mainland; and (3) APHRODITE demonstrates significant advantages than GPCC

50 in calibrating the IMERG, especially over the mountainous regions with complex terrain, e.g., the Tibetan
51 Plateau. Additionally, results of this study suggest that it is a promising and applicable daily calibration
52 algorithm for GPM in generating the future IMERG in either operational scheme or retrospective manner.

53 The AIMERG data record (0.1°/half-hourly, 2000-2015, Asia) is freely available at [http://argi-](http://argi-basic.hihanlin.com:8000/d/d925fecf60/)
54 [basic.hihanlin.com:8000/d/d925fecf60/](http://argi-basic.hihanlin.com:8000/d/d925fecf60/). Additionally, the AIMERG data is also freely accessible at
55 <https://doi.org/10.5281/zenodo.3609352> (for the period from 2000 to 2008) (Ma et al., 2020a) and
56 <http://doi.org/10.5281/zenodo.3609507> (for the period from 2009 to 2015) (Ma et al., 2020b).

57 **Keywords: Precipitation; IMERG; APHRODITE; Calibration; Daily scale; Asia;**

58

59 **1. Introduction**

60 Precipitation is among the most essential hydroclimatic factors, and also most difficult to estimate
61 due to its great small-scale variabilities (Yatagai et al., 2012; Huffman et al., 2019a). High spatio-
62 temporal resolution precipitation dataset with fine quality is essential for various scientific and
63 operational applications, including but not limited to driving the hydrological models, and supporting
64 the predictions of droughts and floods (Beck et al., 2017, 2018). There are mainly two principal
65 approaches for measuring the global precipitation: ground-based gauge observing, and satellite-based
66 remote sensing, which resulting in three mainstreams of global precipitation products, namely gauge

67 analysis precipitation data, satellite-based only precipitation estimates, and satellite-gauge combined
68 precipitation products, based on the consideration that ground-based gauge data are clearly important
69 for anchoring the satellite estimates (Huffman et al., 2007, 2019a).

70 In recent years, a large number of quasi-global satellite precipitation products with various
71 temporal and spatial resolutions have been developed and released to the public, such as the PMW-based
72 CPC Morphing technique (CMORPH) (hereafter, for Acronyms, see the Appendix) (Joyce et al., 2004),
73 and IR-based PERSIANN (Sorooshian et al., 2000) and PERSIANN-CCS (Hong et al., 2004). As the
74 milestone in the satellite-based precipitation measurement process, the TRMM and its successor GPM
75 have developed a flexible framework for generating the most popular precipitation products, TMPA
76 (1998-present, 0.25°/3 hourly) and IMERG (2014-present, 0.1°/half-hourly), as well as the retrospective
77 IMERG (2000-present, 0.1°/half-hourly) from GPM era to TRMM era, which aims at intercalibrating,
78 merging, and interpolating all MW estimates of the GPM constellation, IR estimates, and gauge
79 observations (Huffman et al., 2019b). The “Final run” version of IMERG (hereafter refer to IMERG),
80 incorporating the monthly gauge analysis, provides the state-of-the-art precipitation estimate with finest
81 spatio-temporal resolutions so far, while it still contains large uncertainties, e.g., greatly overestimating
82 the precipitation, at daily and hourly scales from regions to regions, especially over the mountainous
83 areas, such as the Tibetan Plateau, China (Tang et al., 2016; Lu et al., 2019; Xu et al., 2019), which is
84 greatly potentially resulted by the calibration procedures in the process of generating the IMERG.
85 Currently, the IMERG product (following the gauge correction method of TMPA approach) (Huffman

86 et al., 2007) has been produced by anchoring the multi-satellite-only precipitation estimates using the
87 monthly analysis Satellite-Gauge product (1.0°/monthly, 1979 to the present, delayed by about 3 months)
88 from the GPCC (Adler et al., 2003, 2018), therefore, the IMERG performed better at monthly and annual
89 scales than those at finer temporal scales (e.g., daily, hourly).

90 Satellite-based precipitation products have significant advantages in detecting the variations of
91 precipitation at fine spatio-temporal resolutions, especially over the poorly gauged regions. However, as
92 the indirect estimates of precipitation, satellite-based precipitation products are inherently containing
93 regional, seasonal, and diurnal systematic biases and random errors (Ebert et al., 2007), which could be
94 effectively alleviated by anchoring the satellite-only precipitation products using gauge-based
95 observations (Huffman et al., 2007). Therefore, great efforts have been taken on exploring the calibrations
96 on the satellite-only precipitation estimates using gauge analysis. Historically, GPCP has provided the
97 lion's share of the early efforts in the process of developing calibration algorithms for the satellite-only
98 precipitation estimates in generating SG products (2.5°/monthly). For instance, to correct the bias of the
99 multi-satellite only estimates (mainly based on PMW and IR data) on a regional scale, the multi-satellite
100 estimate was firstly multiplied by the ratio of the large-scale (with moving window size 5×5) average
101 gauge analysis to the large-scale average of the multi-satellite estimate, and then the SG estimate was
102 finally derived by combining the gauge-adjusted multi-satellite estimate and the gauge analysis with
103 inverse-error-variance weighting (Huffman et al., 1997; Adler et 2003; Adler 2018). Recently, a two-step
104 strategy was proposed to remove the bias inherent in the multi-satellite only precipitation estimates using

105 PDF matching method and to combine the bias-corrected estimates with the gauge analyses using OI
106 algorithm (Xie and Xiong, 2011; Shen et al., 2014). And a similar improved PDF algorithm was applied
107 to generate the GSMaP data, which was adjusted at the daily scale by the gauge analysis (0.5°/daily) from
108 the CPC (Mega et al., 2014). While GPM IMERG adjusted the multi-satellite precipitation estimates
109 (0.1°/half hourly) at the monthly scale using the ratios between the original monthly multi-satellite-only
110 and the monthly satellite-gauge data, in combination with the original monthly multi-satellite-only and
111 GPCC (1.0°), in the month (Huffman et al., 2019a). There is still much room for exploring the improved
112 algorithms for calibrating the multi-satellite-only precipitation estimates at finer spatiotemporal scales, e.
113 g, 0.25°/daily, which is also one of the next vital focuses by the GPM (Huffman et al., 2019a).

114 As for anchoring the satellite precipitation estimates, the quality and spatio-temporal resolutions of
115 the gauge analysis precipitation data are the key factors. Though the GPCC has developed a series of
116 gauge-based precipitation analysis datasets with the quality and spatio-temporal resolutions continually
117 improved, accurate estimations of precipitation over the land are still greatly difficult with limited
118 networks of rain gauges. In Asia, great efforts also have been mainly paid on generating gauge-analysis
119 precipitation products at the monthly scale (Chen et al., 2002; Mitchell and Jones 2005; Matsuura and
120 Willmott 2009; Schneider et al. 2008), and limited explorations at the daily scale, e.g., Rajeevan and
121 Bhate (2009) explored daily grid precipitation data over India with data from more than 2,500 rain
122 gauges. Meanwhile, significant differences among those products have been reported by Yatagai et al
123 (2005, 2012). To more accurately monitor and predict the Asian hydro-meteorological environment, the

124 APHRODITE project (starting in 2006) aimed at developing the state-of-the-art gridded precipitation
125 datasets at the resolutions of 0.25°/daily covering the entire Asia based on the largest numbers of ground
126 observations from multi-sources. Since the release of APHRODITE products (1951-2015, 0.25°/daily,
127 Last update October 5, 2018), APHRODITE daily grid precipitation data sets have been widely used,
128 and it distinguished from other gauge analysis data by considering the different interpolation schemes
129 and climatology characteristics, especially over the mountainous regions with complex terrain, e.g., the
130 Tibetan Plateau (Yatagai et al., 2012).

131 The aim of this study is to explore the calibration approach at daily scale on the retrospective
132 IMERG data using APHRODITE product, in both TRMM and GPM eras, from 2000 to 2015. Therefore,
133 a new calibration approach, Daily Spatio-Temporal Disaggregation Calibration Algorithm (DSTDCA),
134 is proposed and suggested for the GPM in their future algorithms; meanwhile, a new AIMERG
135 precipitation dataset (0.1°/ half-hourly, 2000-2015, Asia) (Ma et al., 2020a, b) with better quality is to
136 be provided publicly for the Asian applications.

137 **2. Data**

138 **2.1 IMERG**

139 To generate the IMERG product, IMERG focuses on intercalibrating, merging, and interpolating
140 “all” satellite MW-based precipitation estimates, together with MW-calibrated IR-based precipitation
141 estimates, precipitation gauge analyses, and potentially other precipitation estimators at fine spatio-

142 temporal scales for the both TRMM and GPM eras over the entire globe. Currently, IMERG is at its
143 Version 06 stage (https://pmm.nasa.gov/sites/default/files/document_files/IMERG_ATBD_V06.pdf),
144 based on which IMERG has been retrospect to the TRMM era at the end of September, 2019, and
145 IMERG is now available back to June 2000 (0.1°/half-hourly) ([https://pmm.nasa.gov/data-
146 access/downloads/gpm](https://pmm.nasa.gov/data-access/downloads/gpm)). The “Final run” of IMERG combines the GPCC Monitoring product, the V8
147 Full Data Analysis for the majority of the time (currently 1998-2016), and the V6 Monitoring Product
148 from 2017 to the then-present. The Monitoring Product is posted about two months after the month of
149 observations from ~7,000-8,000 stations world-wide, which is relative sparse, especially over the Asia
150 (Schneider et al. 2014, 2018).

151 **2.2 APHRODITE**

152 Since the release of the APHRODITE product (0.25°/Daily, 1951-2007), it has been widely used as
153 one of state-of-the-art daily grid precipitation datasets over the Asia, for hydro-climatological related
154 studies (Yatagai et al., 2012; Menegoz et al., 2013; Sunilkumar et al., 2019). APHRODITE has been
155 demonstrated to replicate ‘ground truth’ observations very well (Duncan and Bigg, 2012) and represents
156 the optimal dataset for analyzing historical precipitation variability and change. Recently, the
157 APHRODITE data has been updated from the former period 1951-2007 to a longer period 1951-2015, in
158 September, 2018, with continuous efforts of quality control (QC) flagging some data (Hamada et al.,

159 2011). The APHRODITE data could be available through the website ([http://aphrodite.st.hirosaki-](http://aphrodite.st.hirosaki-u.ac.jp/download/)
160 [u.ac.jp/download/](http://aphrodite.st.hirosaki-u.ac.jp/download/)).

161 **2.3 CMPA**

162 The China Merged Precipitation Analysis (CMPA, 0.1°/hourly, 2008-2015) has been generated by
163 using hourly rain gauge data at more than 30, 000 automatic weather stations in China, with the
164 combination of the CMORPH precipitation product, and provided by the Chinese Meteorological
165 Administration (<http://data.cma.cn>) (Shen et al., 2014). The OI method was adopted to estimate the areal
166 precipitation distribution based on the gauge observations (Yong et al., 2010), but relative large
167 uncertainty still exists in the interpolated precipitation field particularly over western China with
168 relatively sparse gauge networks. For grid boxes with gauges, the observed precipitation values are
169 exactly the gauge observations or the averaged observations when more than one gauge locate in a grid.

170 **2.4 Point-based rain gauge data from meteorological stations**

171 The hourly rain gauge datasets from 57, 835 national ground stations used in this study, in 2015,
172 were collected from the National Meteorological Information Center of CMA (<http://data.cma.cn>). All
173 the gauge data have undergone strict quality control in three levels, which includes (1) the extreme values'
174 check, (2) internal consistency check, and (3) spatial consistency check (Shen et al., 2010). Most gauges
175 are located over the eastern and southern parts of the Mainland China, and relatively sparse gauge
176 networks are located across the northern and western parts, especially over the Tibetan Plateau. The

177 limited number of gauges could be a source of error in evaluation of satellite precipitation products in
178 such areas (Shen et al., 2014).

179 **2.5 Point-based rain gauge data from hydrological stations**

180 The hourly ground precipitation observations from around 500 hydrological stations (the number of
181 station varied from year to year) used in this study were collected from Hydrology Bureau of Zhejiang
182 Province, southeastern China (<http://data.cma.cn/>). The quality control follows two steps: (1) the datasets
183 are filtered by threshold value after being collected from rain gauges; (2) the outliers are identified through
184 manual processing. With careful data quality control, the rain gauge datasets have satisfying performances
185 on the accuracy and validity.

186 There are five datasets used in this study (refer to Table 1 for a summary of the datasets). IMERG
187 and APHRODITE have been used for generating the AIMERG data, and the others have been used for
188 evaluating and comparing the IMERG and AIMERG at different scales.

189

190 **Table 1.** List of satellite-based, gauge-based, and satellite-gauge combination precipitation products used
 191 in this study.

Short name	Full name	Spatial and temporal sampling	Time period	References
IMERG	Integrated Multi-satellitE Retrievals for Global Precipitation Measurement	0.1°/half-hourly	2000-2015	Huffman et al. (2019b) https://pmm.nasa.gov/data-access/downloads/gpm (last access: 17 January 2020)
APHRODITE	Asian Precipitation Highly Resolved Observational Data Integration Towards Evaluation of Water Resources	0.25°/daily	1951-2015	Yatagai et al. (2012) http://aphrodite.st.hirosaki-u.ac.jp/download/ (last access: 17 January 2020)
CMPA	China Merged Precipitation Analysis	0.1°/hourly	2008-2015	Shen et al. (2014) http://data.cma.cn (last access: 17 January 2020)
	Point-based rain gauge data from meteorological stations	hourly	2015	Shen et al. (2010) http://data.cma.cn (last access: 17 January 2020)
	Point-based rain gauge data from hydrological stations	hourly	2010-2015	Shen et al. (2010) http://data.cma.cn (last access: 17 January 2020)

192

193 **3. Methodology**

3.1 Calibration Procedure of the Daily Spatio-Temporal Disaggregation Calibration

Algorithm, DSTDCA

According to previous evaluations on IMERG (Lu et al., 2019; Xu et al., 2019), there are at least two characteristics resulting its significant overestimations: (1) the amplitude of hourly or half-hourly estimated rainfall rates are significantly amplified by IMERG compared with ground observations, which might be caused by the benchmark of GPCC and GPCP SG data for calibrations, and (2) the IMERG algorithm is generally over detecting precipitation events, resulting a large fraction of false alarm but unreal precipitation events. Therefore, this study selects the APHRODITE data as the benchmark for calibrating IMERG at daily scale, based on the proposed approach, DSTDCA, and the main steps of the DSTDCA are shown as follows:

(1) IMERG data (0.1° /half-hourly) are accumulated to IMERG data at the daily scale (0.1°), which are used to generate the spatial disaggregation weights. As the spatial resolution of APHRODITE data is 0.25° , the moving window size of 3 by 3 is selected, and the daily spatial disaggregation weights (0.1°) based on IMERG is obtained by calculating the ratios between the daily rainfall accumulations at the central grid and the average daily rainfall accumulations in the corresponding 3×3 window. The daily spatial disaggregation weights consider the relative spatial patterns of the precipitation captured by the IMERG;

211 (2) Based on the daily precipitation accumulations of IMERG, the half-hourly temporal
212 disaggregation weights (0.1°) are derived by calculating the ratios between the each half-hourly
213 precipitation estimates and the corresponding daily precipitation estimates. If the daily accumulation
214 estimate is equal to zero, then each half-hourly temporal disaggregation weight is set as zero;

215 (3) As there is a small fraction of grids in APHRODITE with no data at daily scale, the no data grids
216 in APHRODITE data are firstly filled with the data according to its nearest neighbor with effective value;

217 (4) Spatial calibrations: the daily calibrated IMERG using APHRODITE data are obtained by
218 multiplying the spatial disaggregation weights based on IMERG ($0.1^\circ/\text{daily}$) from step (1) by daily
219 APHRODITE data ($0.25^\circ/\text{daily}$) from step (3). In this step, to match the IMERG (0.1°) and APHRODITE
220 (0.25°), the numbers and weights of the APHRODITE grids corresponding to each IMERG pixel are
221 determined, according to the relative spatial locations and coverage relationships between the each pixel
222 of IMERG (0.1°) and the corresponding pixels of APHRODITE (0.25°);

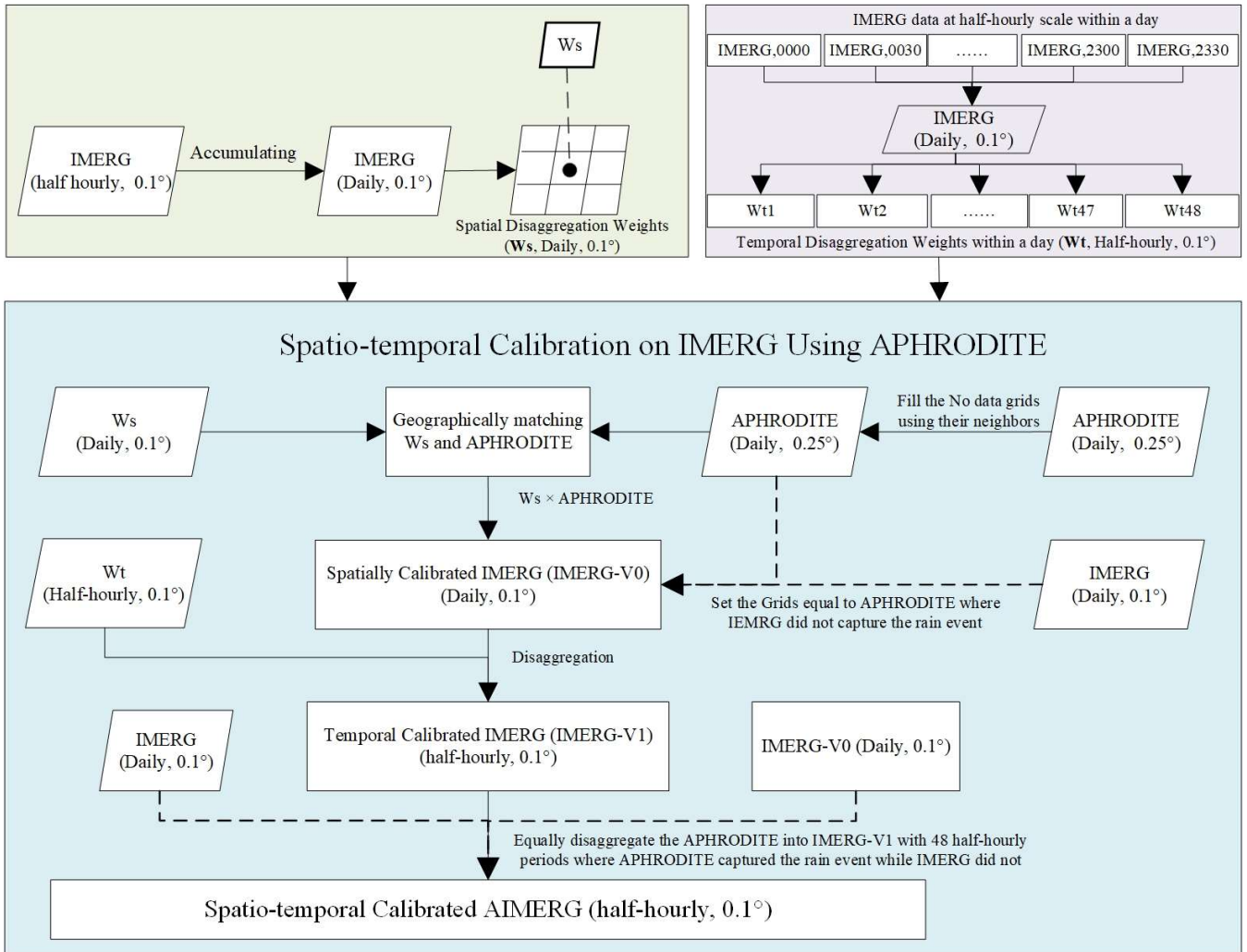
223 (5) Temporal calibrations: the half-hourly calibrated IMERG are obtained by multiplying the half-
224 hourly temporal disaggregation weights ($0.1^\circ/\text{half-hourly}$) from step (2) by the daily calibrated IMERG
225 from step (4);

226 (6) By considering the situations that APHRODITE data captured the precipitation while the IMERG
227 did not, the half-hourly calibrated IMERG is further processed by equally disaggregating the value from

228 the daily APHRODITE data at the corresponding grid into 48 half-hourly periods, which are regarded as
229 the half-hourly calibrated IMERG values in the corresponding day;

230 (7) By considering the situations that IMERG data captured the precipitation while the APHRODITE
231 did not, the 48 half-hourly calibrated IMERG values in corresponding days and locations are all set as
232 zero values, to meet the ground truth observations. And this consideration has been already conducted in
233 the step (4);

234 After all the above-mentioned procedures, the final calibrated AIMERG (0.1° half-hourly) data are
235 obtained by considering both the total precipitation controls and the effective precipitation events
236 measured by the “ground truth” observations by APHRODITE data over the Asia. And the flowchart of
237 the Daily Spatio-Temporal Disaggregation Calibration Algorithm, DSTDCA, could be clearly seen in
238 Figure 1.



240

241

242

243

Figure 1. The flowchart of the Daily Spatio-Temporal Disaggregation Calibration Algorithm, DSTDCA, to generate the AIMERG dataset over the Asia, 2000-2015

3.2 Evaluation Metrics

244 To evaluate the IMERG and its calibrations comprehensively, seven metrics (CC, MAE, BIAS,
 245 RMSE, POD, FAR, CSI) were selected in this study (Tang et al., 2016). Generally, CC is used to describe
 246 the agreements between satellite estimates and gauge observations; MAE, RMSE, and BIAS are used to
 247 indicate the error and bias of satellite estimates compared with gauge observations; and the POD, FAR,
 248 and CSI are used to demonstrate the capabilities to correctly capture the precipitation events of satellite
 249 precipitation estimates against the ground observations. The detailed information of these evaluation
 250 metrics are listed in Table 2.

251 **Table 2** Formulas and perfect values of the evaluation metrics used in this study^a.

Statistic metrics	Equation	Perfect value	Value ranges
Correlation Coefficient (CC)	$CC = \frac{\frac{1}{N} \sum_{n=1}^N (S_n - \bar{s})(G_n - \bar{G})}{\sigma_S \sigma_G}$	1	[-1, 1]
Mean Absolute Error (MAE)	$MAE = \frac{1}{N} \sum_{n=1}^N (S_n - G_n)$	0	(0, +∞)
Relative Bias (BIAS)	$BIAS = \frac{\sum_{n=1}^N (S_n - G_n)}{\sum_{i=1}^n G_n} \times 100\%$	0	(-∞, +∞)
Root Mean Square Error (RMSE)	$RMSE = \sqrt{\frac{1}{N} \sum_{n=1}^N (S_n - G_n)^2}$	0	[0, +∞)
Probability of Detection (POD)	$POD = \frac{n_{11}}{n_{11} + n_{01}}$	1	[0, 1]
False Alarm Ratio (FAR)	$FAR = \frac{n_{10}}{n_{11} + n_{10}}$	0	[0, 1]
Critical Success Index (CSI)	$CSI = \frac{n_{11}}{n_{11} + n_{10} + n_{01}}$	1	[0, 1]

252 ^aNotation: n is the sample numbers; S_n is satellite precipitation estimate; G_n is gauge-based precipitation; σ_G is the standard deviations of
 253 gauge-based precipitation; σ_S is the standard deviations of satellite-based precipitation estimate. n₁₁ is the precipitation event detected by
 254 both gauge and satellite simultaneously; n₁₀ is the precipitation event detected by the satellite but not detected by the gauge; n₀₁ is contrary
 255 to n₁₀; n₀₀ is the precipitation events detected neither by the gauge nor the satellite.

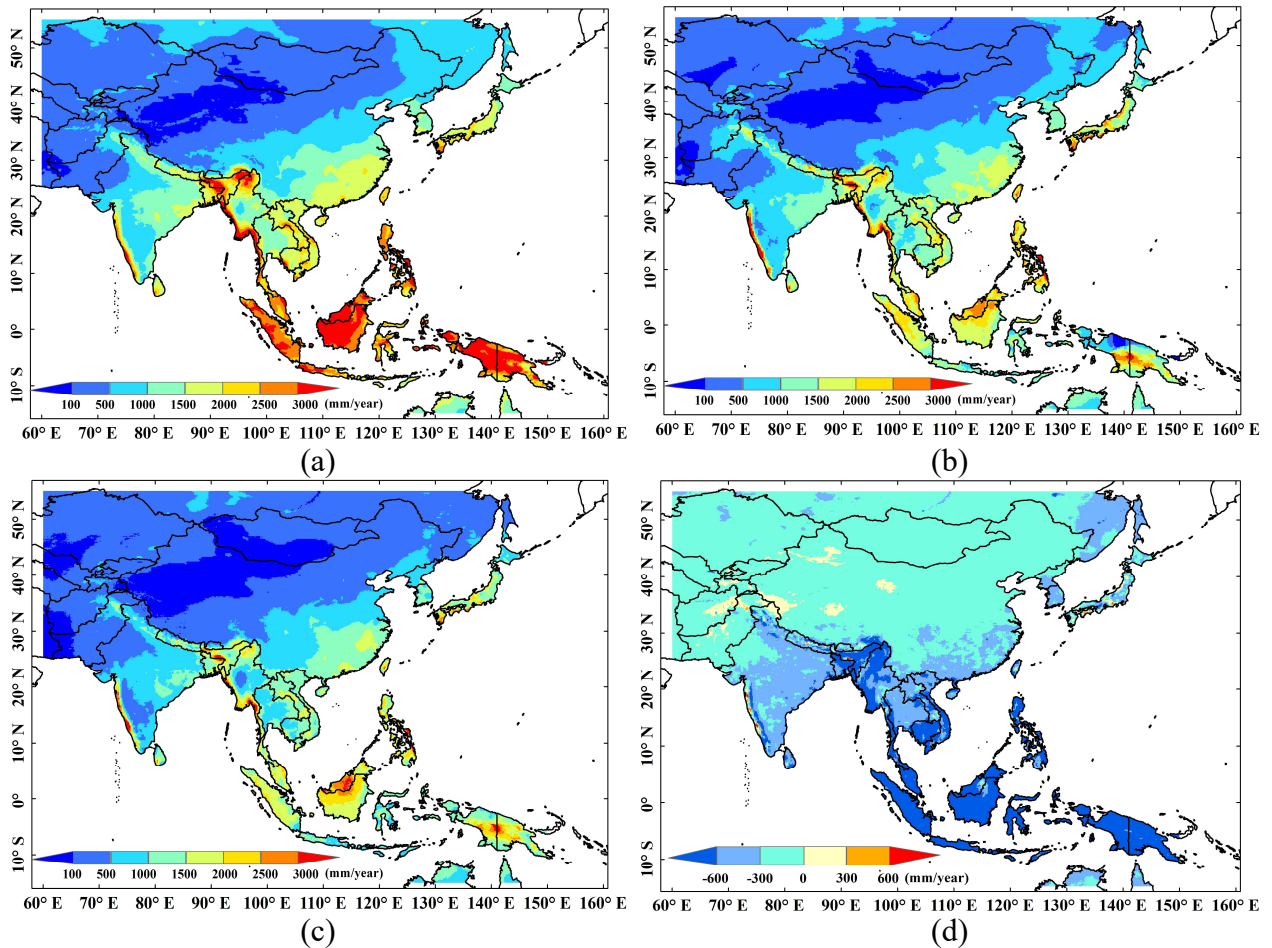
256

257 4. Results

258 4.1 AIMERG Product

259 Generally, both IMERG and APHRODITE share similar spatial patterns with precipitation volumes
260 decreasing from southeast to northwest in Asia, while compared with APHRODITE data (Fig. 2b),
261 IMERG greatly overestimates the precipitation over Arunachal Pradesh, coastal Indochina and Western
262 Ghats, and the Indonesia (Fig. 2a). Corrected by APHRODITE, the spatial patterns and volumes of
263 AIMERG are much more similar to those of APHRODITE, especially along the Himalayas, coastal
264 Indochina and Western Ghats, and the Indonesia (Fig. 2c). Compared with APHRODITE, AIMERG
265 seems floating up and down in terms of the volumes, for instance, AIMERG is larger and smaller than
266 APHRODITE in eastern Indonesia and northeastern Asia, respectively. Though AIMERG is smaller than
267 IMERG over most regions, there are still some areas where the volumes of AIMERG are larger than those
268 of IMERG, e.g., in western Tibetan Plateau (Fig. 2d).

269

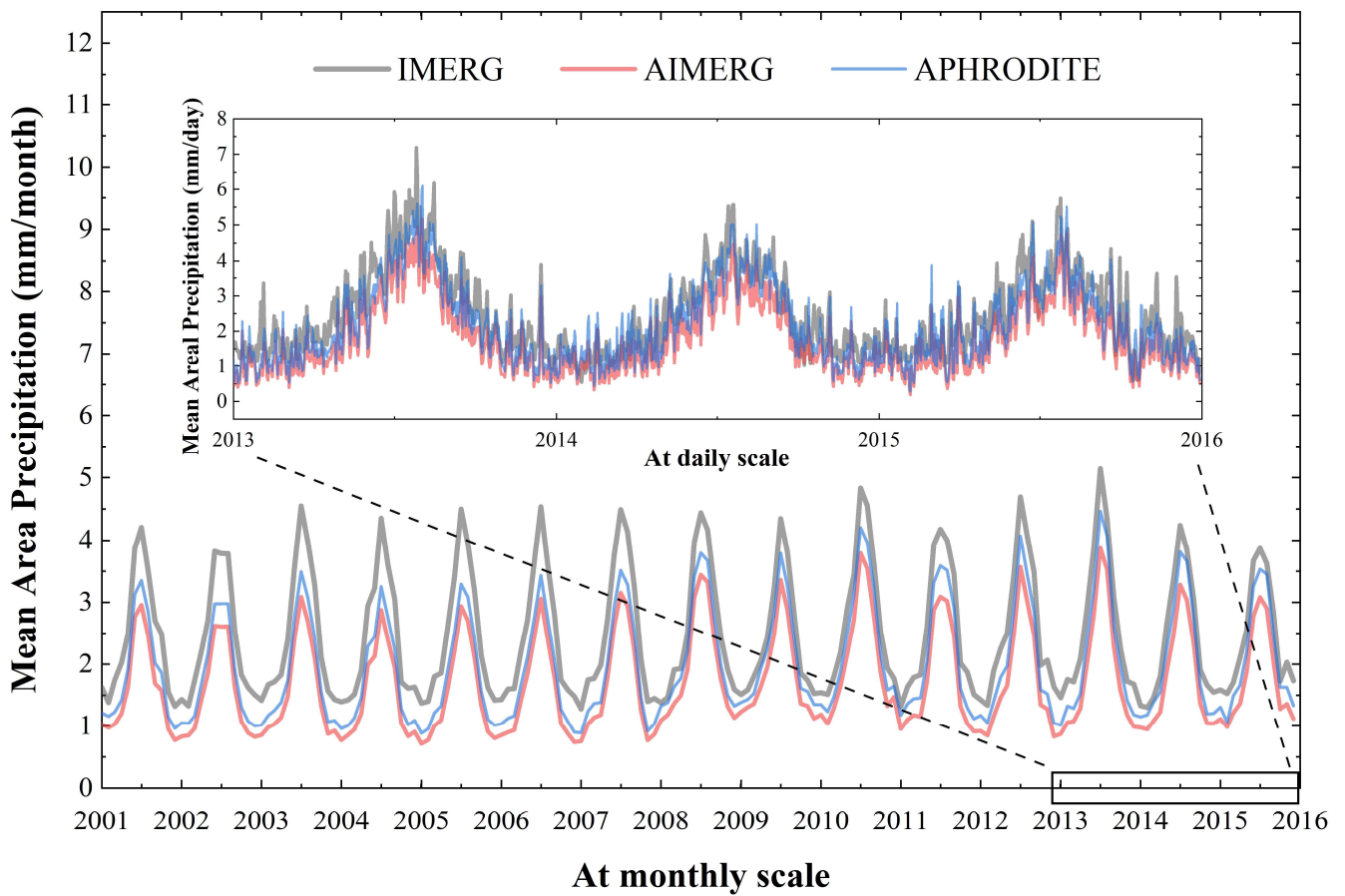


270 Figure 2. Spatial patterns of Asian mean annual gridded precipitation products of (a) IMERG, 0.1°, (b)
 271 APHRODITE, 0.25°, and (c) AIMERG, 0.1°, and (d) AIMERG-IMERG, 0.1°, respectively, during the
 272 period of 2001-2015.

273

274 The temporal patterns of the mean areal precipitation over the Monsoon Asia of the three products
 275 demonstrate that the systematic bias of IMERG is significantly reduced in both dry and wet seasons,

276 shown in Fig. 3. IMERG is around 1.5 times larger than APHRODITE at monthly scale. Though much
277 more close to the APHRODITE, AIMERG is still a little smaller than the APHRODITE, which means
278 the calibration algorithm proposed by this study tends to underestimate the precipitation compared with
279 calibration benchmark, APHRODITE. At daily scale, IMERG is generally larger than APHRODITE,
280 while at some special days, APHRODITE is larger than IMERG, which might result the AIMERG may
281 be also larger than IMERG.



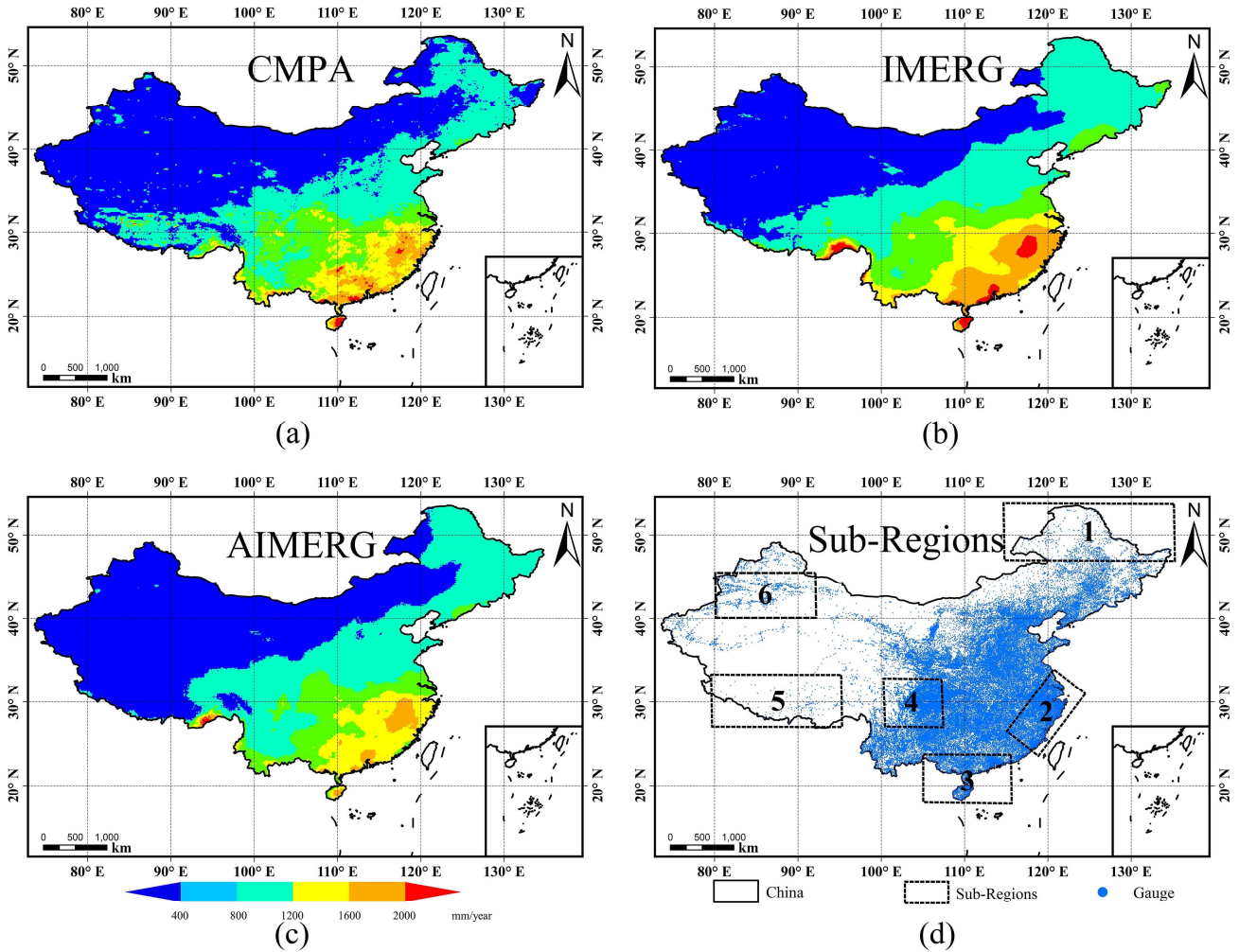
282

283 Figure 3. The temporal variations of mean Asian gridded precipitation products of IMERG, APHRODITE,
284 and AIMERG, respectively, during the period of 2001-2015.

285 **4.2 Assessments on IMERG and AIMERG at national and regional scales**

286 The spatial patterns of CMPA demonstrate much more similar to those of AIMERG, especially in
287 the southeastern China where dense rain gauges are located, while both CMPA and IMERG overestimate
288 the precipitation along the Himalayas where the meteorological gauges are sparse and mainly the satellite-
289 based observations are applied (Fig. 4). Obviously, the IMERG significantly overestimates the
290 precipitation in the southeast coast of China, where typhoons always visit (Fig. 4 b). For deciding the
291 sub-regions (Fig. 4 d), we have mainly considered three aspects: the representative climatic zones in
292 China, the local distributions of the gauge stations, and the complexity of the topography. For instances,
293 Sub-Region 1 represents the high latitude plain in the most north-eastern region of China under a cold
294 climate (left top: 115.0° E, 54.0°N; right bottom: 135.0° E, 47.0°N); Sub-Region 2 represents the south-
295 eastern coastal area of China influenced greatly by the Asian Monsoons (left top: 115.0° E, 26.0°N; left
296 bottom: 119.0° E, 24.0°N; right bottom: 124.0° E, 31.0°N; right top: 120.0° E, 34.0°N); Sub-Region 3
297 represents the most southern region including the island Hainan in the tropical zone (left top: 105.0° E,
298 24.0°N; right bottom: 115.0° E, 18.0°N); Sub-Region 4 represents the inner area of China covering the
299 Yunnan-Kweichow Plateau and Sichuan Basin, under a humid inland climate (left top: 100.0° E, 33.0°N;
300 right bottom: 107.0° E, 27.0°N); Sub-Region 5 represents the most southern Tibetan Plateau along the

301 Himalayas with complex terrains and high elevations above ~ 4000.0 meters (left top: 80.0° E, 33.0° N;
 302 right bottom: 95.0° E, 27.0° N); Sub-Region 6 represents the central Asia with complex terrains covering
 303 the entire Tianshan Mountains in China under an arid inland climate (left top: 80.0° E, 45.0° N; right
 304 bottom: 92.0° E, 40.0° N).

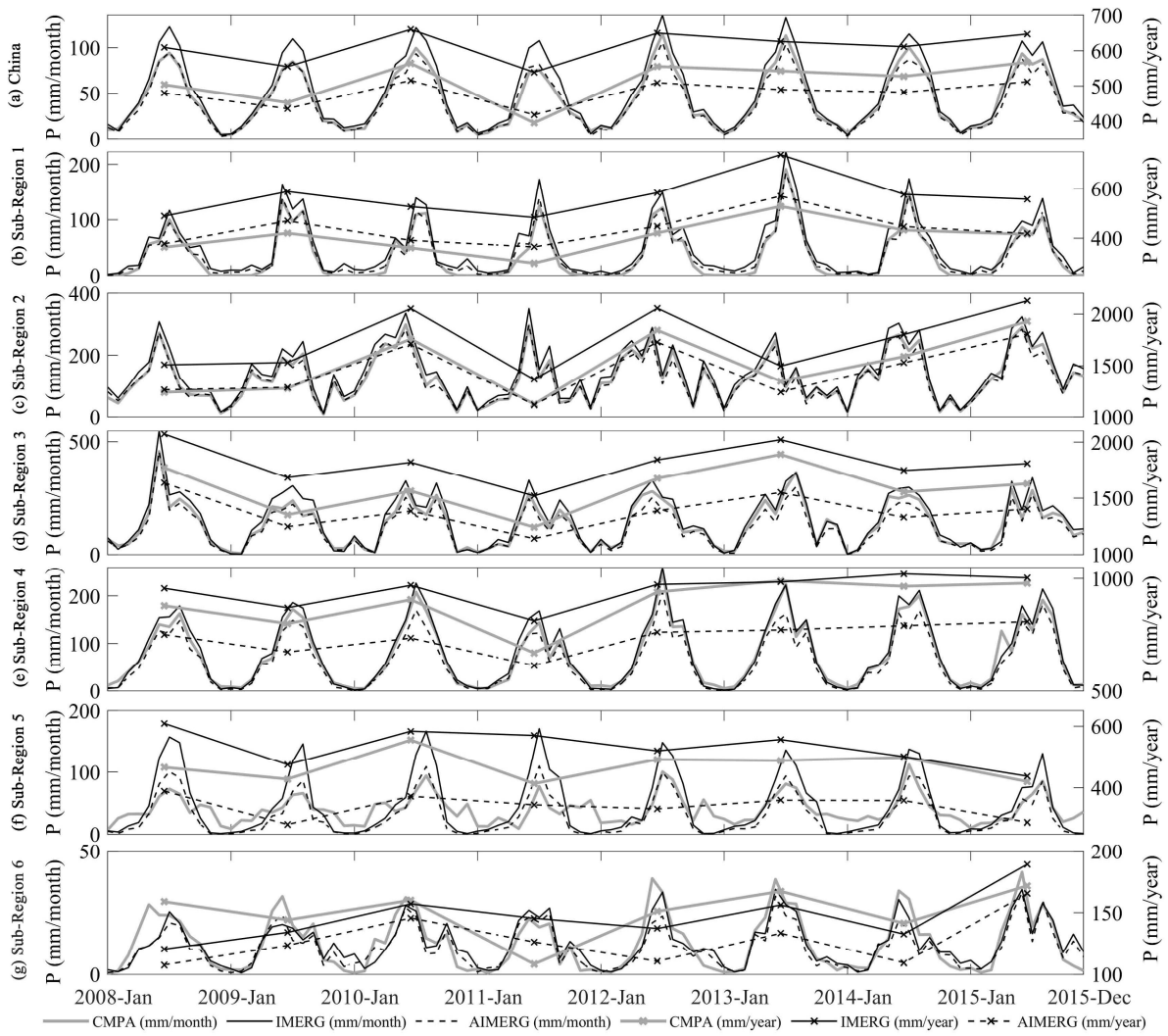


305

306 Figure 4 Spatial patterns of (a) CMPA, (b) IMERG, and (c) AIMERG over China Mainland From 2008
307 to 2015, and (d) the spatial distributions of more than 50,000 automatic meteorological stations in China
308 Mainland. The accurate boundary information of the Sub-Regions: Sub-Region 1 (left top: 115.0° E,
309 54.0°N; right bottom: 135.0° E, 47.0°N); Sub-Region 2 (left top: 115.0° E, 26.0°N; left bottom: 119.0°
310 E, 24.0°N; right bottom: 124.0° E, 31.0°N; right top: 120.0° E, 34.0°N); Sub-Region 3 (left top: 105.0°
311 E, 24.0°N; right bottom: 115.0° E, 18.0°N); Sub-Region 4 (left top: 100.0° E, 33.0°N; right bottom: 107.0°
312 E, 27.0°N); Sub-Region 5 (left top: 80.0° E, 33.0°N; right bottom: 95.0° E, 27.0°N); Sub-Region 6 (left
313 top: 80.0° E, 45.0°N; right bottom: 92.0° E, 40.0°N).

314

315 The magnitudes of IMERG, AIMERG, and CMPA are compared at national and regional scale
316 over the China Mainland from 2008 to 2015 (Fig. 5). Generally speaking, CMPA and AIMERG are almost
317 same, and are significantly smaller than IMERG at both annual and monthly scales, additionally, CMPA
318 is still a little larger than AIMERG over the China Mainland, which could be possibly resulted from the
319 use of satellite observations in the CMPA and IMERG (Fig. 6a). The overall situations of the three
320 product in sub-region 1 and 2 are similar with those over the China Mainland (Fig. 6 b-c), while both
321 CMPA and IMERG are both significantly larger than AIMERG (Fig. 6 d-f). In sub-region 6, the Tianshan
322 Mountains, CMPA is almost even larger than IMERG, which indicates that large uncertainties should be
323 focused on sub-region 6 (Fig. 6 g).

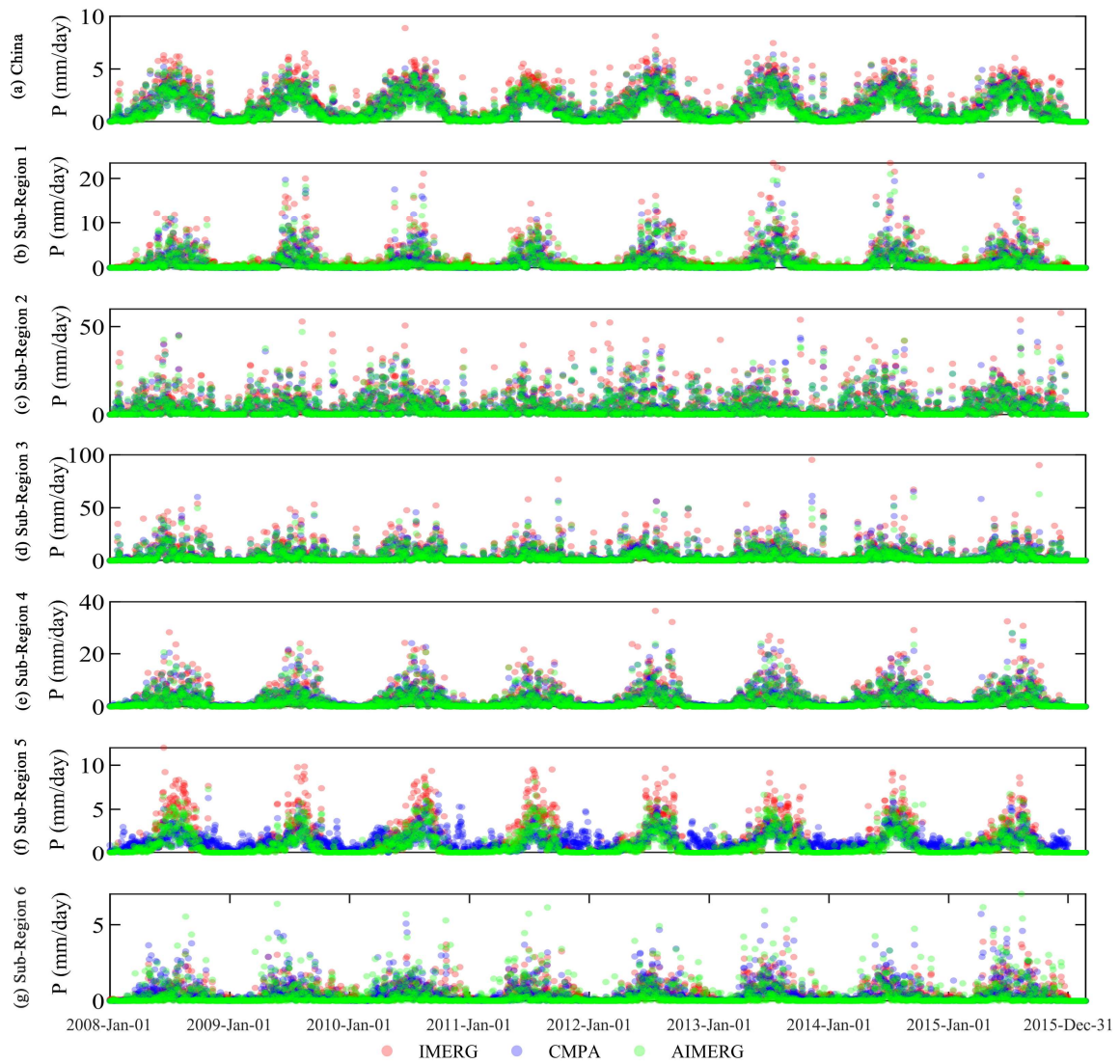


324

325 Figure 5. The temporal patterns of mean areal precipitation of the IMERG, CMAP, and AIMERG, over
 326 China Mainland and sub-regions from 2008 to 2015, at monthly and annual scales.

327 As this study aims to propose a new algorithm for calibrating the IMERG product at the daily scale,
328 the daily spatial patterns of IMERG, CMAPA, and AIMERG have also been explored, which generally
329 agree with those of IMERG, CMAPA, and AIMERG at monthly scale (Fig. 6). In mountainous region,
330 along the Himalayas, with relatively small precipitation, CMAPA is greatly larger and smaller than the
331 other two products (both IMERG and AIMERG) in dry seasons and wet seasons respectively (Fig. 6 f).
332 One phenomenon should be noted that the CMAPA seems abnormal along the Himalayas, which might be
333 resulted by the limited ground observations used in CMAPA, shown in Fig. 4d, while APHRODITE data
334 integrate large numbers of ground observations from the neighbor countries, such as India, Nepal, Bhutan,
335 providing valuable information for retrieving high quality precipitation product around the Tibetan
336 Plateau (Yatagai, 2012). Calibrated by APHRODITE at daily scale, AIMERG is significantly smaller
337 than IMERG and CMAPA at both annual and monthly scale, while there are also some situations that
338 AIMERG is larger than IMERG and CMAPA at daily scale, for example in sub-region 6, over the Tianshan
339 mountains.

340



341

342 Figure 6. The temporal patterns of mean areal precipitation of the IMERG, CMPA, and AIMERG, over

343

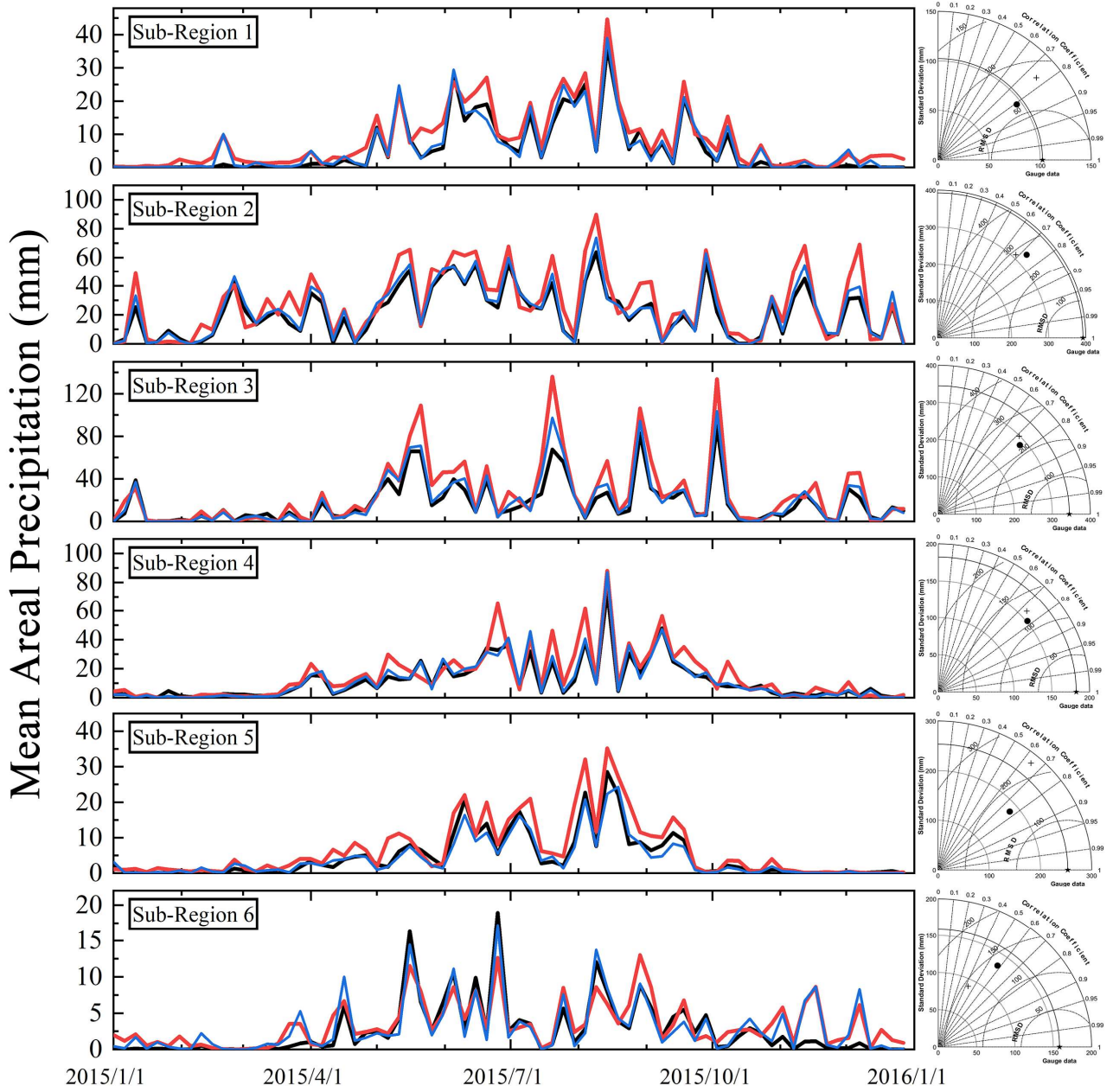
China Mainland and sub-regions from 2008 to 2015, at daily scale.

344

345 Hourly ground observation data from more than 50,000 meteorological stations were used to assess
346 the quality of the IMERG and its calibrations, AIMERG, over the six sub-regions, in 2015 (Fig. 7). The
347 temporal patterns and volumes of mean areal precipitation by AIMERG and ground observations are
348 almost same, while IMERG is generally larger than AIMERG and ground observations. Meanwhile, the
349 IMERG still has the problems in overestimating and underestimating the precipitation in dry seasons
350 (relatively large precipitation occurring) and wet seasons (relatively small precipitation happening),
351 respectively, for example in sub-region 6, over the Tianshan Mountains. In terms of quantitative indices
352 (Standard deviation, RMSD, and CC), AIMERG generally outperforms the IMERG against the ground
353 observations, especially in sub-region 5, along the Himalayas, which indicates that the ground information
354 from the neighbor countries integrated into the APHRODITE data greatly benefits the calibration results,
355 AIMERG.

356

— Gauge Data — IMERG — AIMERG + IMERG ● AIMERG

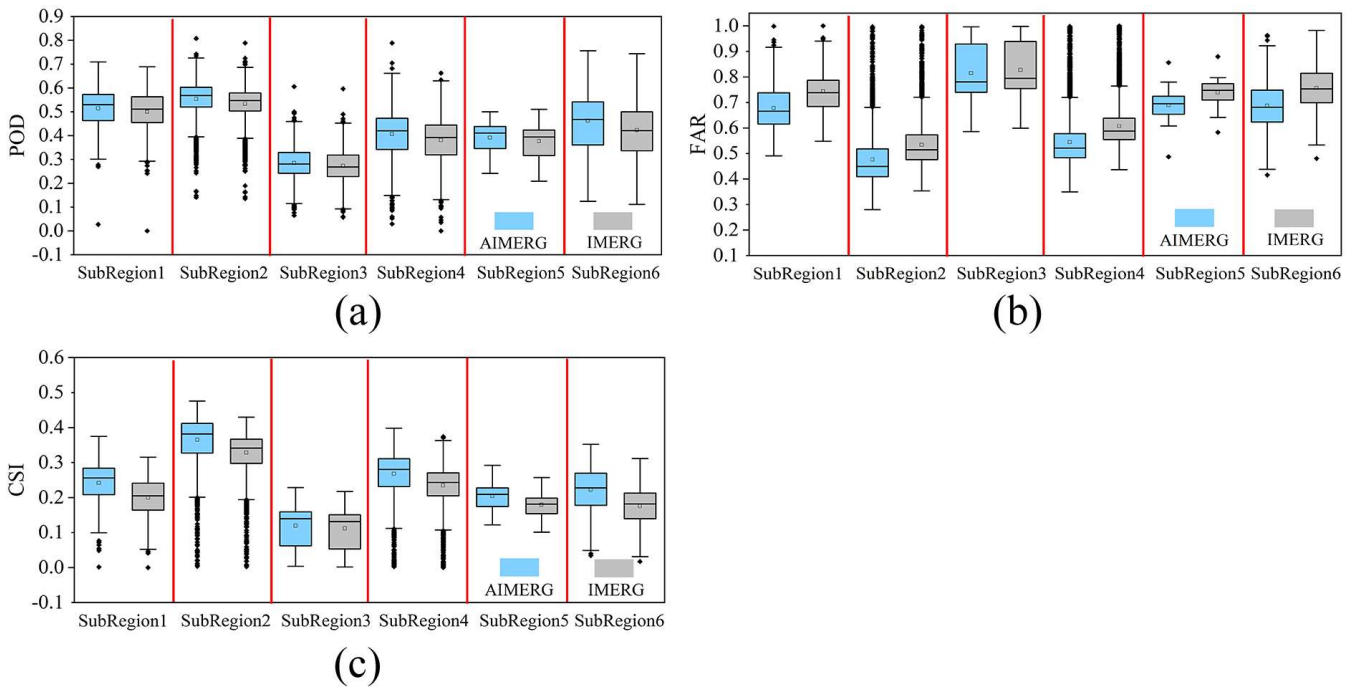


357

358 Figure 7. The temporal patterns and the volumes of IMERG, ground observations, and AIMERG, in six
359 sub-regions at daily scale; and the Taylor diagrams of performances on IMERG and AIMERG against
360 ground observations in terms of centered root-mean-square difference, correlation coefficient and
361 standard deviation in the six sub-regions at hourly scale, in 2015.

362

363 Figure 8 illustrates the numerical distributions of contingency statistics for IMERG and AIMERG,
364 at hourly scale, in six sub-regions, 2015. Generally, the POD values of AIMERG are larger than those of
365 IMERG (Fig. 8a), and FAR values of AIMERG are overall smaller than those of IMERG in each sub-
366 regions (Fig. 8b), which results the better performances of the comprehensive index, CSI, combining both
367 the characteristics of POD and FAR, in each sub-regions (Fig. 8c). Additionally, both the IMERG and
368 AIMERG perform best in sub-region 2, and worst in sub-region 3.



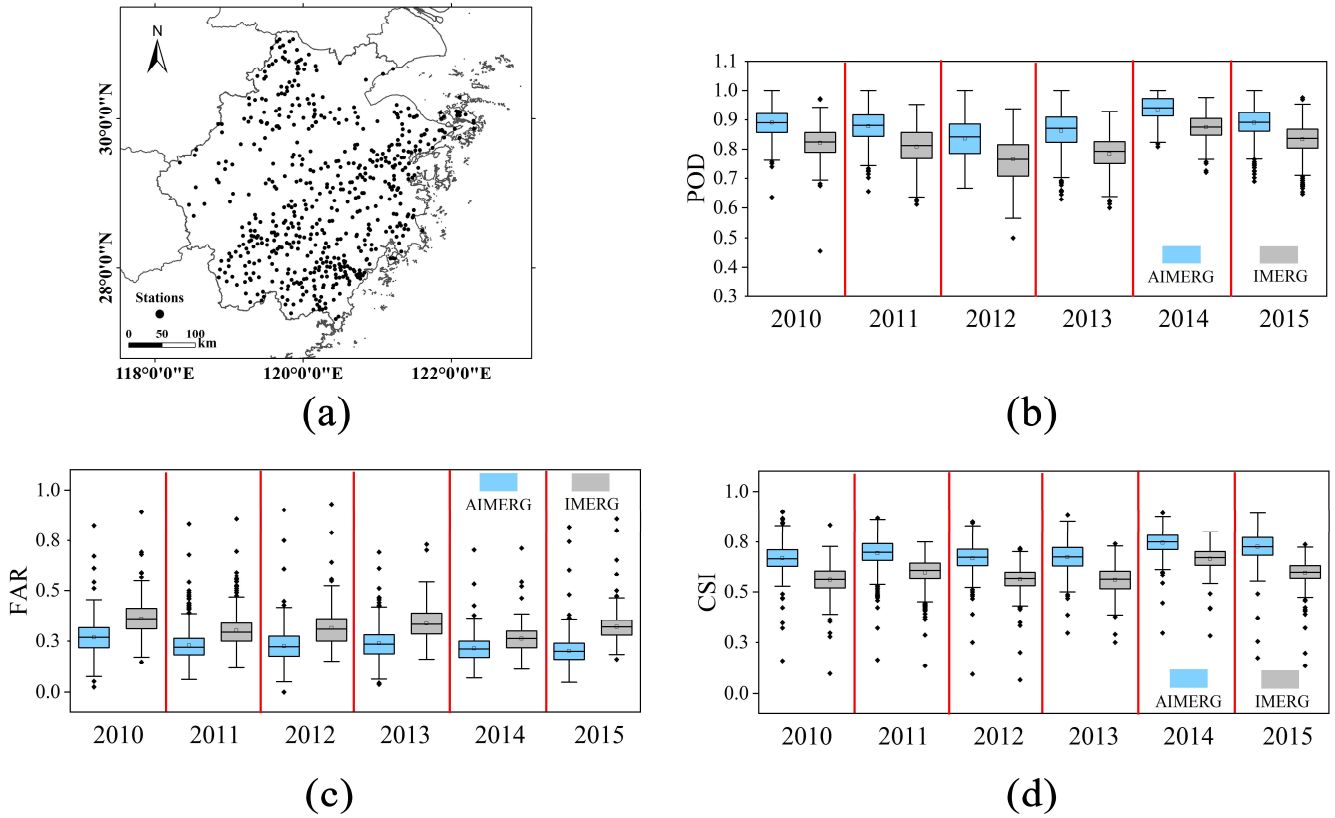
369

370 Figure 8. The boxplots demonstrate diagnose of IMERG and AIMERG against the ground observations
 371 from the meteorological stations, at hourly scale, in six sub-regions, 2015.

372

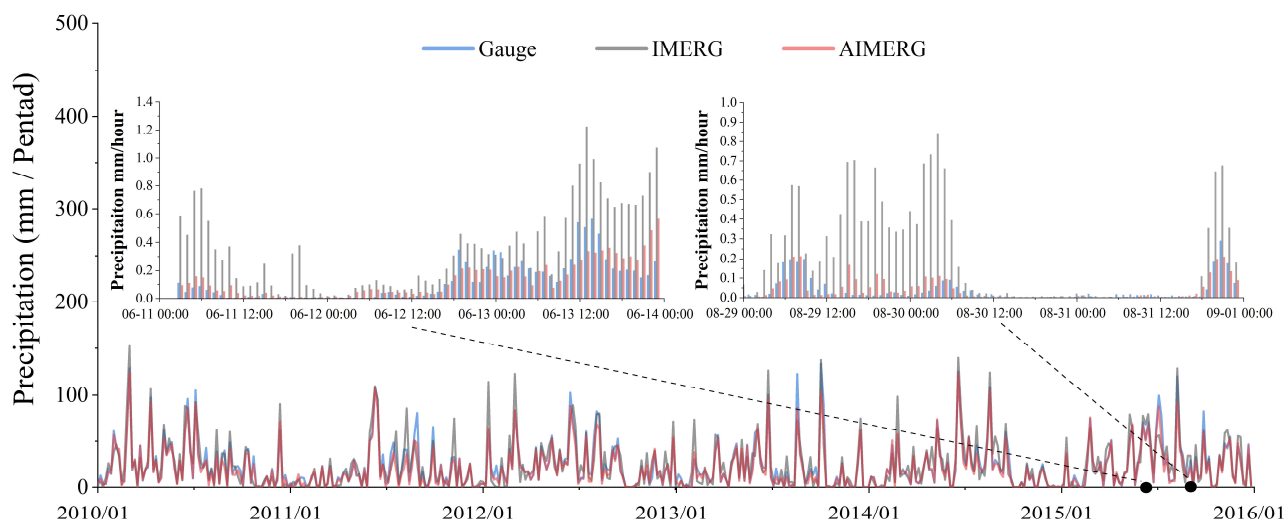
373 To assess the quality of the IMERG and AIMERG, entirely independent precipitation data from
 374 around 500 hydrological stations, at hourly scale, from 2010 to 2015, were applied, which are relatively
 375 even distributed in Zhejiang province (Fig. 9a). The POD values of AIMERG (~ 0.9) are general larger
 376 than those of IMERG (~ 0.8), while the FAR values of AIMERG (~ 0.3) are significantly smaller than
 377 those of IMERG (~ 0.4), which results in the overall capabilities of AIMERG to capture the precipitation

378 events are improved more than 10%, compared with IMERG, in terms of the CSI. The relative smaller
 379 POD values and larger FAR values of IMERG in the Zhejiang province, southeastern coast of China,
 380 might be one of the potential drawbacks in accurately estimating the precipitation both qualitatively and
 381 quantitatively.



382
 383 Figure 9. The boxplots demonstrate diagnose of IMERG and AIMERG against the ground observations
 384 from hydrological stations, respectively, at hourly scale, in Zhejiang province, 2010-2015.

385 From the temporal patterns of mean areal precipitation of IMERG, AIMERG, and ground
 386 observations from hydrological stations, in Zhejiang province, 2010-2015 (Fig. 10), IMERG is general
 387 larger than both AIMERG and ground observations. For instance, the IMERG significantly overestimates
 388 the precipitation with up to ten times than that of AIMERG and ground observations, such as in the typical
 389 periods, 0 a.m., June, 11 – 0 a.m., June, 14, 2015, and 0 a.m., Aug, 29 – 0 a.m., Sep, 1, 2015. Additionally,
 390 both the temporal patterns and the magnitudes of AIMERG are almost same with those of ground
 391 observations, compared with those of IMERG. Meanwhile, in some pentads with the heavy rain events,
 392 both AIMERG and ground observations are larger than IMERG.



393
 394 Figure 10. The temporal patterns of mean areal precipitation of IMERG, AIMERG, and the ground
 395 observations from the independent hydrological stations, at daily/hourly scale, in Zhejiang province,
 396 2010-2015.

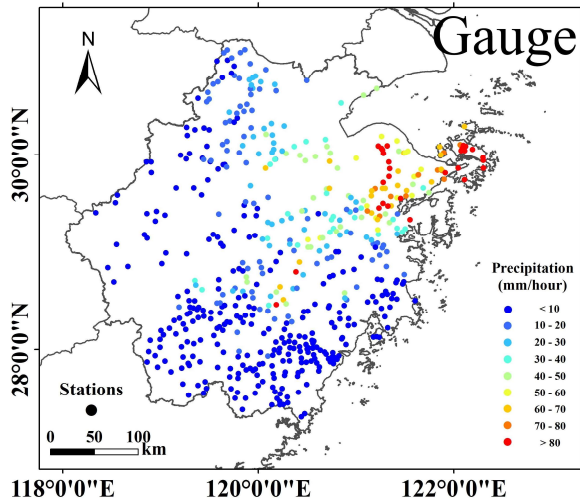
397 **4.3. The performances of AIMERG and other products in capturing the heavy rainfall event**

398 One of the primary aims of the satellite-based precipitation estimates is to provide the high quality
399 rainfall information, accurately capturing both the spatial patterns and volumes of the rainfall, at hourly
400 scale during the heavy rainfall events. Recently, Tang et al (2020) has conducted a comprehensive
401 comparison of GPM IMERG with other nine state-of-the-art high resolution precipitation products, six
402 satellite-based precipitation products (TRMM 3B42, 0.25°/3 hour; CMORPH, 0.25°/3 hour; PERSIANN-
403 CDR, 0.25°/1 day; GSMaP 0.1°/1 hour; CHIRPS, 0.05°/1 day; SM2RAIN, 0.25°/1 day) and three
404 reanalysis datasets (ERA5, ~0.25°/1 hour; ERA-Interim, ~0.75°/3 hour; MERRA2~0.5° × 0.625°/1 hour)
405 from 2000 to 2018, and found that the IMERG product generally outperformed other datasets, except the
406 Global Satellite Mapping of Precipitation (GSMaP), which was adjusted at the daily scale by the gauge
407 analysis (0.5°/daily) from the CPC (Mega et al., 2014). Therefore, we have quantitatively and horizontally
408 compared the AIMERG with GSMaP, as well as the IMERG against ground observations.

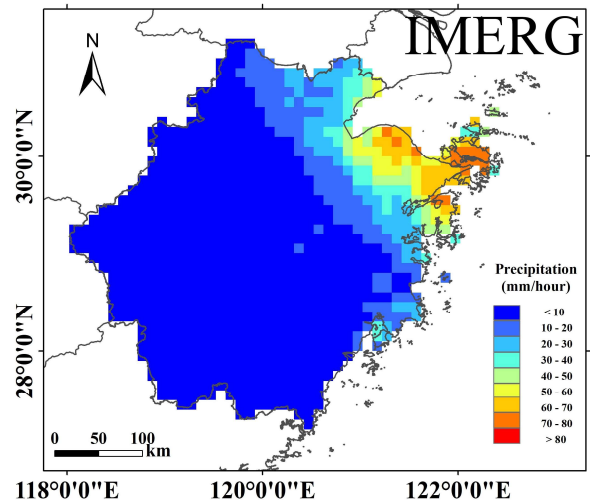
409 In this study, the typhoon, Chan-hom, is selected as an example for assessing the quality of
410 AIMERG and other products, occurred in the typical period 0 a.m., – 11 a.m., July, 11, 2015, in Zhejiang
411 province (Fig. 11 a-d). Generally, the spatial patterns of the IMERG, GSMaP, AIMERG are similar with
412 those of the ground observations, with the increasing volumes of rainfall from southwest to northeast. In
413 terms of the three satellite-based rainfall estimates, IMERG underestimates the rainfall greater than those
414 of GSMaP and AIMERG, in the heavy rainfall events (Fig. 11 b), with largest regions in the southwestern

415 Zhejiang (rainfall < 10 mm/hour). Though GSMaP estimates the rainfall greater than IMERG in both
416 spatial coverages and volumes (Fig. 11 c), the AIMERG provides much more details than GSMaP,
417 especially over the northeastern Zhejiang Province (Fig. 11 c). As pointed out by various studies (e.g.,
418 Tang et al., 2020), the satellite-based precipitation products generally overestimate the volumes in small
419 rainfall events, but underestimate the volumes during the heavy rainfall events. From this aspect,
420 AIMERG outperforms the GSMaP as well as the original IMERG, owing to the daily calibrations using
421 the ground observations.

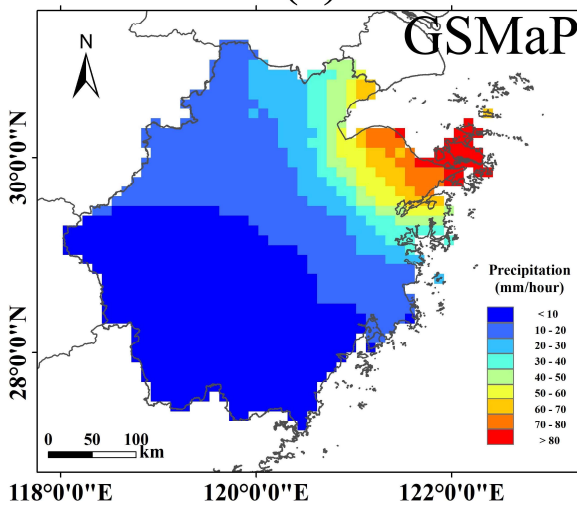
422



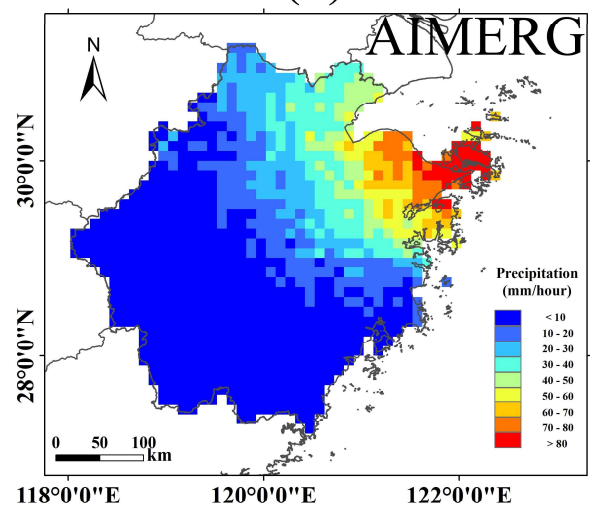
(a)



(b)



(c)

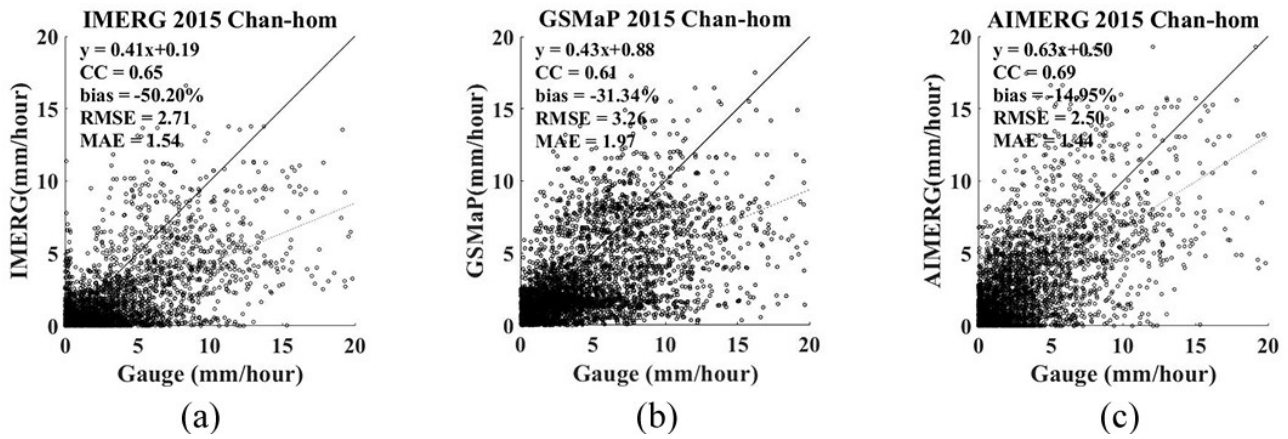


(d)

423

424 Figure 11. The spatial patterns of precipitation measured by (a) IMERG, (b) GSMaP, and (c) AIMERG,
 425 during the typhoon, Chan-hom, occurred in the typical period 0 a.m., – 11 a.m., July, 11, 2015, in Zhejiang
 426 Province.

428 To quantitatively assess the performances of the AIMERG, GSMaP, and IMERG, they are also
429 evaluated against the ground observations, during the typhoon, Chan-hom, occurred in the typical period
430 0 a.m., – 11 a.m., July, 11, 2015, in Zhejiang province (Fig. 12 a-c). From the statistics, not only the
431 systematic bias of IMERG (around -50%) is significantly improved, with the bias of AIMERG around -
432 10%, but also the random errors of IMERG (RMSE \sim 2.7 mm/hour, MAE \sim 1.5 mm/hour) are also reduced,
433 compared with AIMERG (RMSE \sim 2.5 mm/hour, MAE \sim 1.4 mm/hour), which meant the calibrations
434 using APHRODITE on IMERG improved the abilities of original IMERG product to more accurately
435 estimate the quantitative precipitation volumes, especially in heavy rainfall events (Fig. 12 a and c).
436 Meanwhile, AIMERG significantly overwhelms GSMaP in terms of both bias and random errors. For
437 instance, GSMaP underestimates the precipitation (bias \sim -31%) twice as large as AIMERG (bias \sim -15%),
438 and the random errors of GSMaP (MAE \sim 1.97 mm/hour, RMSE \sim 3.26 mm/hour) are also significantly
439 larger than those of AIMERG (MAE \sim 1.44 mm/hour, RMSE \sim 2.50 mm/hour) (Fig. 12 b and c).
440 Compared with the original IMERG, though the random errors of GSMaP are relatively larger, the bias
441 of GSMaP (\sim -31%) is significantly smaller than that of the original IMERG (\sim -50%), which owes to the
442 calibrations on the GSMaP at the daily scale (Fig. 12 a and b). In future, we also encourage researchers
443 to comprehensively evaluate and compare the AIMERG with other high resolution precipitation products
444 at various spatio-temporal scales.



445

446 Figure 12. The scatterplots of (a) IMERG, (b) GSMaP, and (c) AIMERG against ground observations
 447 during the typhoon, Chan-hom, occurred in the typical period 0 a.m., – 11 a.m., July, 11, 2015, in Zhejiang
 448 Province.

449 The extent of the AIMERG could cover the Northern Eurasia, Middle East, Monsoon Asia, and
 450 Japan. This study mainly evaluated the AIMERG in the China Mainland, which calls for Asia wide
 451 evaluations in the future to assess both the algorithm and the corresponding precipitation product. For
 452 regions with relative dense rain gauge networks, it is better to quantitatively and horizontally evaluate
 453 the AIMERG and other precipitation estimates against ground observations, using statistical evaluations
 454 (Lu et al., 201; Xu et al., 2019; Tang et al., 2020), for example, in Japan, and Monsoon India. While for
 455 regions with relative sparse rain gauge networks, it is optimal to horizontally compare the performances
 456 and abilities of AIMERG with those of other products in precipitation-related application fields, e.g., in
 457 hydrological simulations at basin scales (Ma et al., 2018).

458

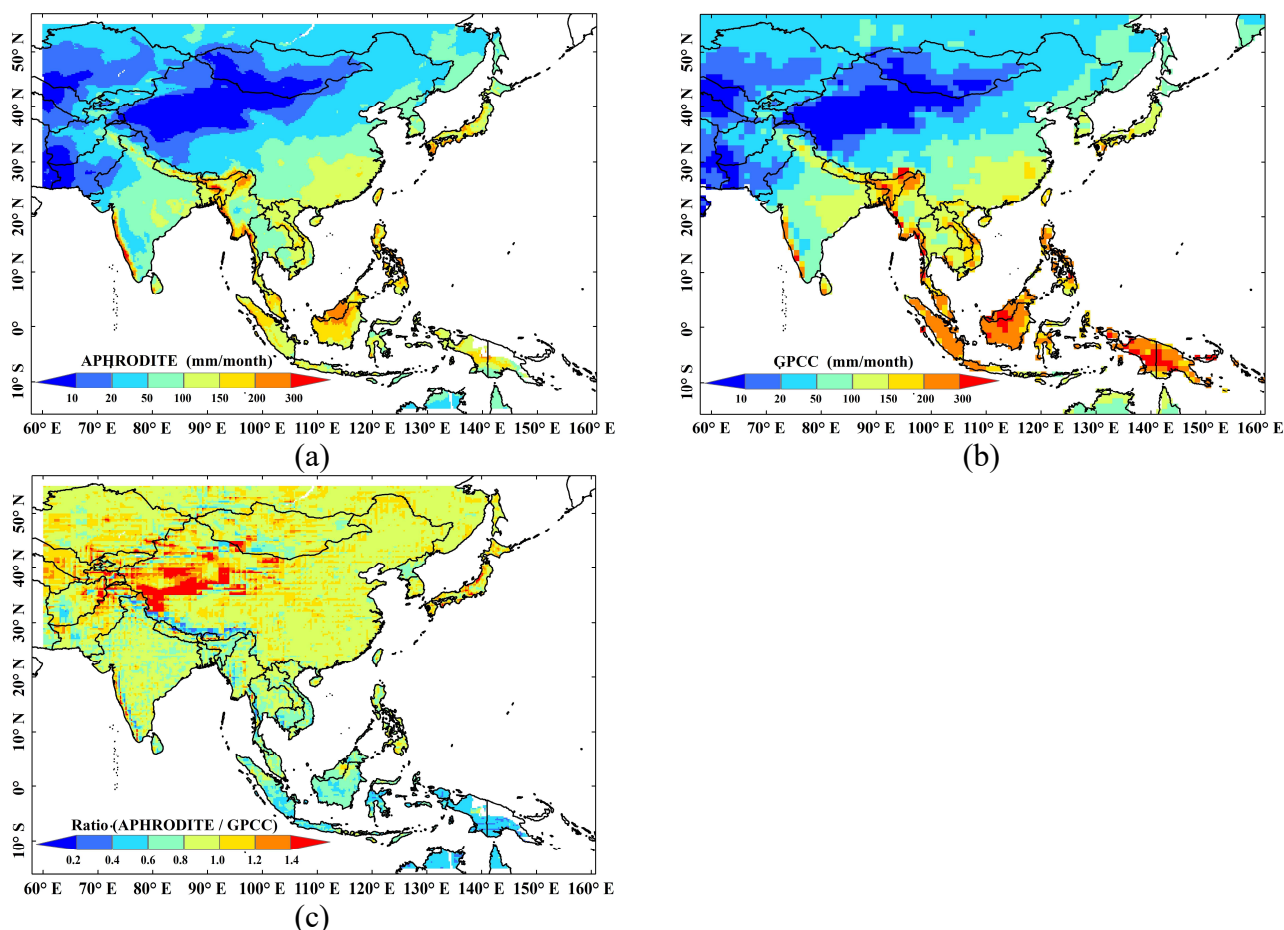
459 **5. Discussions**

460 **5.1. The potential drawbacks in processing the IMERG product**

461 From the document of “Algorithm Theoretical Basis Document (ATBD) Version 06” for
462 generating the final IMERG product (Huffman et al., 2019a), we find that there are mainly two steps in
463 the process: the first step is to derive the multi-satellite-only precipitation inversion estimates, and the
464 second step is to calibrate the multi-satellite-only precipitation estimates using the interpolated
465 precipitation product based on ground observations, e.g., GPCC (1.0°/monthly). As lacking mature
466 calibration algorithm for calibrating the multi-satellite-only precipitation estimates at daily scale, the
467 current IMERG-Final product are only calibrated using the GPCC at monthly scale. The two aims of this
468 study are to provide (1) a spatio-temporal calibration algorithm (DSTDCA) for anchoring the satellite-
469 based precipitation estimates at daily scale, and (2) a new precipitation product with finer quality, namely
470 AIMERG (half-hourly, $0.1^\circ \times 0.1^\circ$, 2000-2015, Asia) (Ma et al., 2020a, b), for Asian researcher. For
471 anchoring the IMERG final product, we introduce the APHRODITE data (daily, $0.25^\circ \times 0.25^\circ$, 2000-
472 2015, Asia), which were interpolated based on the ground observations from the large numbers of rain
473 gauges. Though the general spatial patterns of monthly mean precipitation estimates from both
474 APHRODITE and GPCC, from 1951 to 2015, are similar, the volumes of them demonstrate significant
475 differences, especially along the Himalayas, coastal Indochina and Western Ghats, and the Indonesia (Fig.

476 13 a-b). To much more clearly demonstrate the relative values of GPCC and APHRODITE, the spatial
477 patterns of the ratio of monthly mean values of APHRODITE to those of GPCC are illustrated in Fig. 13
478 c, from which we find that GPCC significantly overestimates the precipitation in the tropical rain range
479 along the Indonesia, and along the southern Himalayas with complex terrain, while it significantly
480 underestimates the precipitation in the north western Tibetan Plateau and Middle East, compared with the
481 ground “truth” product, APHRODITE. Illustrated by Fig. 13, the GPCC plays vital roles in the final
482 IMERG product, and the introduction of APHRODITE on calibrating the IMERG would be greatly
483 benefiting the quality of the AIMERG.

484

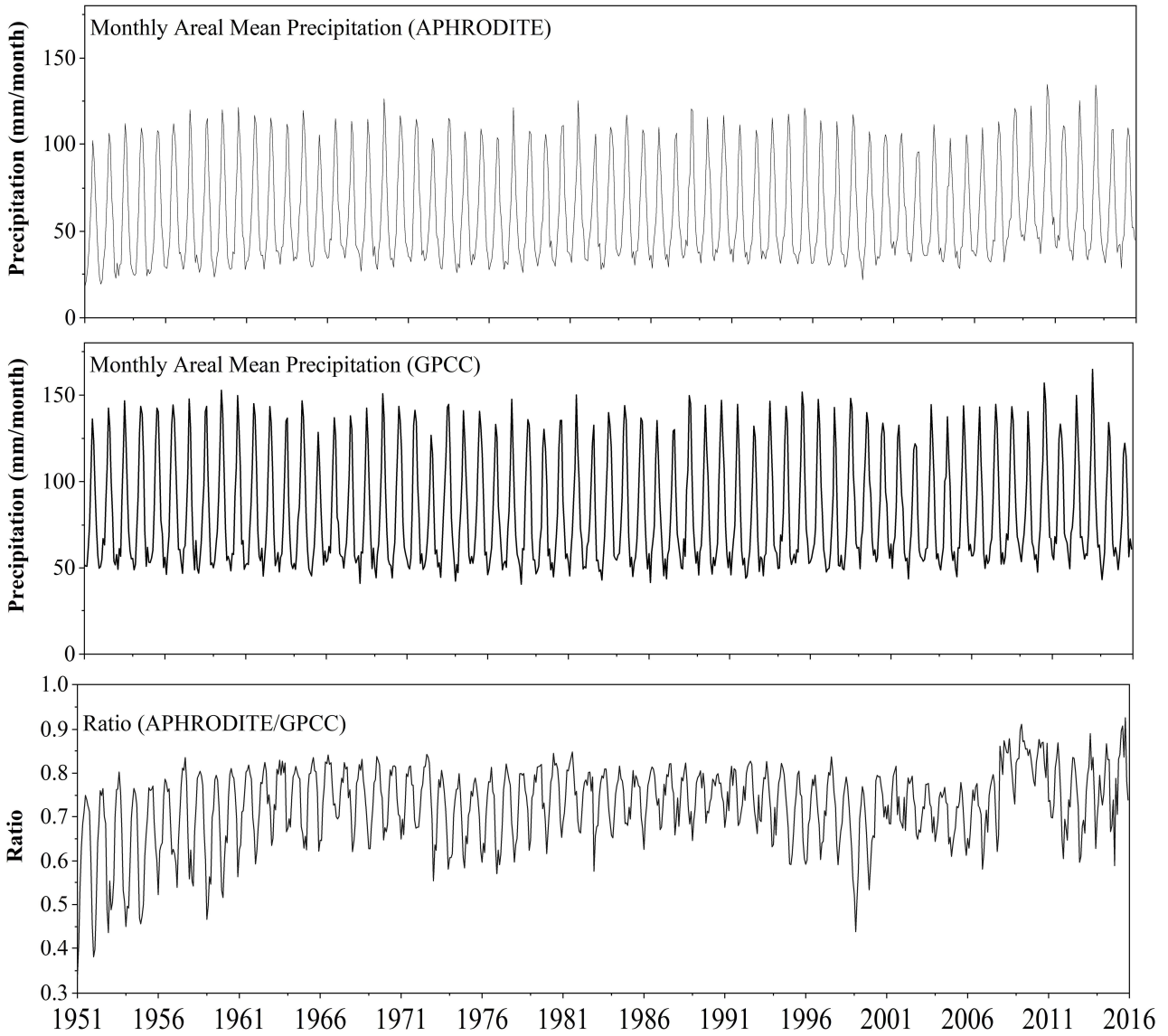


485 Figure 13. The spatial patterns of the monthly mean precipitation of (a) APHRODITE and (b) GPCC, and
 486 (c) Ratios between monthly mean values of APHRODITE and GPCC, over the Asia in the period from
 487 1951 to 2015.

488 There are mainly two kinds of errors in the multi-satellite-only precipitation product, including
 489 systematic bias and random errors (Shen et al., 2014). As seen in the above-mentioned results, the random
 490 errors of the AIMERG are alleviated by using the APHRODITE data compared with IMERG (e.g., Fig.

491 4-13). In terms of the systematic errors, we compared the monthly Asian mean precipitation estimates of
492 both APHRODITE and GPCC, from 1951 to 2015 (Fig. 14). The monthly Asian mean precipitation of
493 APHRODITE varies between ~ 25 mm/month and ~ 100 mm/month, while those of GPCC ranges from
494 ~ 50 mm/month and ~ 150 mm/month, which results the ratios of APHRODITE to GPCC fluctuate
495 significantly from ~ 0.2 to ~ 0.9 , with average value ~ 0.7 , which means that the GPCC at least
496 overestimates the precipitation more than $\sim 30\%$, compared with the APHRODITE. Therefore, the
497 introduction of APHRODITE data would greatly reduce the systematic errors of the IMERG final product,
498 over the Asia.

499



500

501 Figure 14. The temporal patterns of monthly areal mean precipitation of (a) APHRODITE and (b)
 502 GPCC, and monthly (c) ratio values of corresponding areal mean APHRODITE/GPCC, 1951-2015.

503

504 **5.2. The controls on the range of the spatial weights based on IMERG**

505 As demonstrated in the document of the “ATBD” (Huffman et al., 2019a), gauge information is
506 introduced into the original multi-satellite-only half-hourly data to generate the final IMERG product.
507 Firstly, the ratio between the monthly accumulation of half-hourly multi-satellite-only field and the
508 monthly satellite-gauge field is calculated, then each half-hourly field of multi-satellite-only precipitation
509 estimates in the corresponding month is multiplied by the ratio field to generate the half-hourly calibrated
510 IMERG. After various experiments, the ratio values between the monthly satellite-gauge and the monthly
511 accumulation of half-hourly multi-satellite-only fields is limited to the range [0.2, 3] (Huffman et al.,
512 2019a). The cap of 3 is decided due to the value of 2 (used in TRMM V6) was too restrictive. Meanwhile,
513 the cap of 3 is finally applied because it performed better in matching the two accumulations than that of
514 other larger values, for instance, the cap of 4 resulted in introducing unrealistic shifts to histogram of half-
515 hourly precipitation rates for the month. Additionally, early in TRMM the lower bound of 0.5 was applied,
516 which suggested a smaller value of the lower bound allows matching between the two accumulations
517 without creating the egregious high snapshot values when the upper bound was expanded too far.

518 Inspired by the range of the ratio values between the monthly satellite-gauge and the monthly
519 accumulation of half-hourly multi-satellite-only fields in generating IMERG, we consider the range [0,
520 1.5] of the daily spatial disaggregation weights in this study is reasonable after careful checking the
521 distributions of the spatial disaggregation weights. The lower bound of 0 was selected based on the

522 consideration if the IMERG did not capture the daily precipitation event, then the spatial disaggregation
523 weight is still equal to zero, which agrees as most as possible to the original IMERG. While there are at
524 least two reasons for setting the upper bound of the spatial disaggregation weights as 1.5: (1) most
525 numerical values of spatial disaggregation weights are in the range [0, 1.5], and (2) there are obvious
526 anomalies in the final calibrated AIMERG, especially along the coastal regions and edges of the specific
527 precipitation event coverages, where the values of the spatial disaggregation weights are larger than 1.5.
528 Though the range [0, 1.5] of spatial disaggregation weights was applied to obtain the final AIMERG in
529 this study, we also consider that this is still an open-ended issue.

530 **5.3. The advantages of APHRODITE data in anchoring the multi-satellite-only precipitation** 531 **product**

532 It has been a great challenge to obtain precipitation estimates over the Tibetan Plateau and its
533 surroundings, as there are very limited ground observations in this region, especially in its western parts
534 (Ma et al., 2017). Incorporating a uniform precipitation gauge analysis is important and critical for
535 controlling the bias that typifies the satellite precipitation estimates, e.g., using GPCC for TMPA and
536 IMERG (Huffman et al., 2019a). Those projects (e.g., GPCC, TRMM, GPM) demonstrate that even
537 monthly gauge analyses contribute significant improvements on the satellite-only precipitation estimates,
538 at least for some regions in some seasons. Primarily explorations at CPC suggested substantial
539 improvements in the bias corrections using daily gauge analysis, especially for regions, where there is a

540 dense network of gauges (Mega et al., 2014). Foreseeably, GPM would try their best to calibrate the GPM
541 multi-satellite-only precipitation estimates at finer spatio-temporal scales (e.g., 0.25°/daily) worldwide.

542 Currently, GPCC has been adopted to calibrate the TRMM TMPA and GPM IMERG at monthly
543 scale. The Deutscher Wetterdienst (DWD) Global Precipitation Climatology Centre (GPCC) was
544 established in 1989 to provide high-quality precipitation analyses over land based on conventional
545 precipitation gauges from ~7,000-8,000 stations world-wide (Schneider et al. 2014, 2018). And two
546 GPCC products were applied in the IMERG, the V8 Full Data Analysis for the majority of the time
547 (currently 1998-2016), and the V6 Monitoring Product from 2017 to the then-present. Compared with
548 GPCC, APHRODITE has inherently advantages with significantly larger numbers of ground observations
549 and finer spatio-temporal resolutions, over the Asia. APHRODITE projects aim at collecting as most
550 gauge information as possible from the Asian countries. There are mainly three kinds of gauge
551 information sources used in APHRODITE analysis, the GTS-based data, data precompiled by other
552 projects or organizations, and APHRODITE's own collection. More detailed information on the
553 APHRODITE' data sources could be found at the website (<http://www.chikyu.ac.jp/precip/>) and the
554 research of Yatagai (2012). Compared with the GPCC with the limited ground observations in and around
555 the Tibetan Plateau in China, the neighboring countries provide plenty of ground observations in the
556 APHRODITE data, in mountainous regions, and semi-arid and arid regions. Additionally, the spatio-
557 temporal resolutions of APHRODITE (0.25°/daily) are finer than those of GPCC (1.0°/monthly).
558 Therefore, APHRODITE has significant advantages in calibrating the IMERG data at daily scale.

559

560 **6. Data Availability**

561 The AIMERG data record (0.1°/half-hourly, 2000-2015, Asia) is freely available at [http://argi-](http://argi-basic.hihanlin.com:8000/d/d925fecf60/)
562 [basic.hihanlin.com:8000/d/d925fecf60/](http://argi-basic.hihanlin.com:8000/d/d925fecf60/). Additionally, the AIMERG data is also freely accessible at
563 <https://doi.org/10.5281/zenodo.3609352> (for the period from 2000 to 2008) (Ma et al., 2020a) and
564 <http://doi.org/10.5281/zenodo.3609507> (for the period from 2009 to 2015) (Ma et al., 2020b).

565

566 **7. Conclusions**

567 As the milestone in the satellite-based precipitation measurement process, the TRMM and its
568 successor GPM generate the most popular and the state-of-the-art satellite precipitation products for both
569 water cycle related scientific researches and applications, TMPA (1998-present, 0.25°/3 hourly) and
570 IMERG (2014-present, 0.1°/half-hourly), as well as the retrospective IMERG (2000-present, 0.1°/half-
571 hourly) from GPM era to TRMM era. In this study, focusing on the potential drawbacks in generating
572 IMERG and its recently updated retrospective IMERG (finished in July, 2019), which were only
573 calibrated at monthly scale using limited ground observations, GPCC (1.0°/monthly), resulting the
574 IMERG with large systematic bias and random errors, we introduce another daily gauge analysis product,
575 APHRODITE (Last update October 5, 2018), to calibrate the IMERG at 0.25°/daily scale. Compared with

576 GPCP, APHRODITE has inherently advantages with significantly larger numbers of ground observations
577 and finer spatio-temporal resolutions (0.25°/daily), over the Asia.

578 We have proposed a new algorithm (Daily Spatio-Temporal Disaggregation Calibration Algorithm,
579 DSTDCA) for calibrating IMERG at daily scale, and provided a new AIMERG precipitation dataset
580 (0.1°/half-hourly, 2000-2015, Asia) (Ma et al., 2020a, b) with better quality, calibrated by APHRODITE
581 at daily scale for the Asian applications. And the main conclusions include but not limited to: (1) the
582 proposed daily calibration algorithm is effective in considering the advantages from both satellite-based
583 precipitation estimates and the ground observations; (2) AIMERG performs better than IMERG at
584 different spatio-temporal scales, in terms of both systematic biases and random errors, over the China
585 Main land; and (3) APHRODITE demonstrates significant advantages than GPCP in calibrating the
586 IMERG, especially over the mountainous regions with complex terrain, e.g., the Tibetan Plateau.
587 Additionally, results of this study suggests that it is a promising and applicable daily calibration algorithm
588 for GPM in generating the future IMERG in either operational scheme or retrospective manner.

589

590 **Author Contributions**

591 Dr. Ziqiang Ma designed and organized the manuscript. Drs. Jintao Xu, Siyu Zhu, Jun Yang and
592 Yuanjian Yang prepared the related materials and run the models for generating AIMERG and the related
593 assessments. Dr. Guoqiang Tang and Prof. Zhou Shi made contributions on the scientific framework of

594 this study and discussed the interpretation of results. Prof. Yang Hong co-advised this study. All authors
595 discussed the results and commented on the manuscript.

596

597 **Competing interests**

598 The authors declare they have no competing financial interests.

599 **Acknowledgments**

600 This study was financially supported by the Key R&D Program of Ministry of Science and
601 Technology, China (Grant No. 2018YFC1506500); the National Natural Science Foundation of China
602 (Grant No. 41901343); The Second Tibetan Plateau Scientific Expedition and Research (STEP) program
603 (grant no. 2019QZKK0105); the China Postdoctoral Science Foundation (No. 2018M630037, and
604 2019T120021); the National Natural Science Foundation of China (Grant No. 91437214); the Open Fund
605 of the State Key Laboratory of Remote Sensing Science, China (Grant No. OFSLRSS201909), the State
606 Key Laboratory of Resources and Environmental Information System, China.

607 The contribution of the data providers is also greatly appreciated, including the Chinese
608 Meteorological Data Sharing Service System (<http://cdc.nmic.cn/home.do>), the APHRODITE data
609 provider (<http://aphrodite.st.hirosaki-u.ac.jp/download/>), and the IMERG data provider
610 (<https://pmm.nasa.gov/data-access/downloads/gpm>).

611

612 **References**

613 Adler, R. F., Huffman, G. J., Chang, A., Ferraro, R., Xie, P., Janowiak, J., Rudolf, B., Schneider, U.,
614 Curtis, S., Bolvin, D., Gruber, A., Susskind, J., Arkin, P., and Nelkin, E.: The Version-2 Global
615 Precipitation Climatology Project (GPCP) Monthly Precipitation Analysis (1979–Present), *J.*
616 *Hydrometeorol.*, 4, 1147–1167, [https://doi.org/10.1175/1525-](https://doi.org/10.1175/1525-7541(2003)004<1147:TVGPCP>2.0.CO;2)
617 [7541\(2003\)004<1147:TVGPCP>2.0.CO;2](https://doi.org/10.1175/1525-7541(2003)004<1147:TVGPCP>2.0.CO;2), 2003.

618 Adler, R.F., Sapiiano, M., Huffman, G.J., Wang, J.-J., Gu, G., Bolvin, D.T., Chiu, L., Schneider, U.,
619 Becker, A., Nelkin, E.J., Xie, P., Ferraro, R., and Shin, D.-B.: The Global Precipitation Climatology
620 Project (GPCP) Monthly Analysis (New Version 2.3) and a Review of 2017 Global
621 Precipitation, *Atmos.*, 9(4), 138, <https://doi.org/10.3390/atmos9040138>, 2018.

622 Beck, H. E., van Dijk, A. I. J. M., Levizzani, V., Schellekens, J., Miralles, D. G., Martens, B., and Roo,
623 A. d.: MSWEP: 3-hourly 0.25° global gridded precipitation (1979–2015) by merging gauge,
624 satellite, and reanalysis data, *Hydrol. Earth Syst. Sci.*, 21, 589-615, [https://doi.org/10.5194/hess-21-](https://doi.org/10.5194/hess-21-589-2017)
625 [589-2017](https://doi.org/10.5194/hess-21-589-2017), 2017.

626 Beck, H. E., Wood, E. F., Pan, M., Fisher, C. K., Miralles, D. G., van Dijk, A. I. J. M., McVicar, T. R.,
627 and Adler, R. F.: MSWEP V2 Global 3-Hourly 0.1° Precipitation: Methodology and Quantitative

628 Assessment, *Bull. Amer. Meteorol. Soc.*, 100, 473-500, <https://doi.org/10.1175/BAMS-D-17->
629 0138.1, 2018.

630 Chen, M., Xie, P., Janowiak, J., and Arkin, P.: Global Land Precipitation: A 50-yr Monthly Analysis
631 Based on Gauge Observations, *J. Hydrometeorol.*, 3, 249-266, <https://doi.org/10.1175/1525->
632 7541(2002)003<0249:GLPAYM>2.0.CO;2, 2002.

633 Duncan, J. M. A., and Biggs, E. M.: Assessing the accuracy and applied use of satellite-derived
634 precipitation estimates over Nepal, *Appl. Geogr.*, 34, 626–638,
635 <https://doi.org/10.1016/j.apgeog.2012.04.001>, 2014.

636 Ebert, E. E., Janowiak, J. E., and Kidd, C.: Comparison of Near-Real-Time Precipitation Estimates from
637 Satellite Observations and Numerical Models, *Bull. Amer. Meteorol. Soc.*, 88, 47-64,
638 <https://doi.org/10.1175/BAMS-88-1-47>, 2007.

639 Hamada, A., Arakawa, O., and Yatagai, A.: An automated quality control method for daily rain-gauge
640 data, *Global Environmental Research*, 15, 183-192, http://www.airies.or.jp/journal_15-2eng.html,
641 2011.

642 Hong, Y., Hsu, K.-L., Sorooshian, S., and Gao, X.: Precipitation Estimation from Remotely Sensed
643 Imagery Using an Artificial Neural Network Cloud Classification System, *J. Appl. Meteorol.*, 43,
644 1834-1853, <https://doi.org/10.1175/JAM2173.1>, 2004.

645 Huffman, G. J., Adler, R. F., Arkin, P., Chang, A., Ferraro, R., Gruber, A., Janowiak, J., McNab, A.,
646 Rudolf, B., and Schneider, U.: The Global Precipitation Climatology Project (GPCP) Version 1 data
647 set, *Bull. Am. Meteorol. Soc.*, 78, 5-20, [https://doi.org/10.1175/1520-](https://doi.org/10.1175/1520-0477(1997)078<0005:TGPCPG>2.0.CO;2)
648 [0477\(1997\)078<0005:TGPCPG>2.0.CO;2](https://doi.org/10.1175/1520-0477(1997)078<0005:TGPCPG>2.0.CO;2), 1997.

649 Huffman, G. J., Bolvin, D. T., Nelkin, E. J., Wolff, D. B., Adler, R. F., Gu, G., Hong, Y., Bowman, K. P.,
650 and Stocker, E. F.: The TRMM Multisatellite Precipitation Analysis (TMPA): Quasi-Global,
651 Multiyear, Combined-Sensor Precipitation Estimates at Fine Scales, *J. Hydrometeorol.*, 8, 38-55,
652 <https://doi.org/10.1175/JHM560.1>, 2007.

653 Huffman, G. J., Bolvin, D. T., Braithwaite, D., Hsu, K., Joyce, R., Kidd, C., Nelkin, E. J., Sorooshian, S.,
654 Tan, J., and Xie, P.: NASA Global Precipitation Measurement (GPM) Integrated Multi-satellitE
655 Retrievals for GPM (IMERG), Algorithm Theoretical Basis Document (ATBD) Version 06,
656 NASA/GSFC, Greenbelt, MD, USA, 38pp., 2019a.

657 Huffman, G. J., E.F. Stocker, D.T. Bolvin, E.J. Nelkin, and Jackson Tan: GPM IMERG Final
658 Precipitation L3 Half Hourly 0.1 degree x 0.1 degree V06, Greenbelt, MD, Goddard Earth Sciences
659 Data and Information Services Center (GES DISC), [https://doi.org/10.5067/GPM/IMERG/3B-](https://doi.org/10.5067/GPM/IMERG/3B-HH/06)
660 [HH/06](https://doi.org/10.5067/GPM/IMERG/3B-HH/06), 2019b.

661 Joyce, R. J., Janowiak, J. E., Arkin, P. A., and Xie, P.: CMORPH: A Method that Produces Global
662 Precipitation Estimates from Passive Microwave and Infrared Data at High Spatial and Temporal

- 663 Resolution, J. Hydrometeorol., 5, 487-503, <https://doi.org/10.1175/1525->
664 7541(2004)005<0487:CAMTPG>2.0.CO;2, 2004.
- 665 Lu, H., Ding, L., Ma, Z., Li, H., Lu, T., Su, M., and Xu, J.: Spatiotemporal Assessments on the Satellite-
666 Based Precipitation Products From Fengyun and GPM Over the Yunnan-Kweichow Plateau, China,
667 Earth Space Sci., 7, e2019EA000857, <https://doi.org/10.1029/2019EA000857>, 2020.
- 668 Mega, T., Ushio, T., Kubota, T., Kachi, M., Aonashi, K., and Shige, S.: Gauge adjusted global satellite
669 mapping of precipitation (GSMaP_Gauge), in: 2014 XXXIth URSI General Assembly and
670 Scientific Symposium (URSI GASS), Beijing, China, 17-23 August 2014,1–4. 2014.
- 671 Ménégoz, M., Gallée, H., and Jacobi, H. W.: Precipitation and snow cover in the Himalaya: from
672 reanalysis to regional climate simulations, Hydrol. Earth Syst. Sci., 17, 3921–3936,
673 <https://doi.org/10.5194/hess-17-3921-2013>, 2013.
- 674 Ma, Z., Jin, X., Zhu, S., Tang, G., Yang, Y., Shi, Z., and Hong, Y.: AIMERG: a new Asian precipitation
675 dataset (0.1°/half-hourly, 2000-2008) by calibrating GPM IMERG at daily scale using
676 APHRODITE [Data set], Zenodo, <https://doi.org/10.5281/zenodo.3609352>, 2020.
- 677 Ma, Z., Jin, X., Zhu, S., Tang, G., Yang, Y., Shi, Z., and Hong, Y.: AIMERG: a new Asian precipitation
678 dataset (0.1°/half-hourly, 2009-2015) by calibrating GPM IMERG at daily scale using
679 APHRODITE [Data set], Zenodo, <https://doi.org/10.5281/zenodo.3609507>, 2020.
- 680 Ma, Z., Shi, Z., Zhou, Y., Xu, J., Yu, W., and Yang, Y.: A spatial data mining algorithm for downscaling

681 TMAPA 3B43 V7 data over the Qinghai–Tibet Plateau with the effects of systematic anomalies
682 removed, *Remote Sens. Environ.*, 200, 378-395, <https://doi.org/10.1016/j.rse.2017.08.023>, 2017.

683 Ma, Z., Tan, X., Yang, Y., Chen, X., Kan, G., Ji, X., Lu, H., Long, J., Cui, Y., and Hong, Y.: The First
684 Comparisons of IMERG and the Downscaled Results Based on IMERG in Hydrological Utility
685 over the Ganjiang River Basin, *Water-sui*, 10(10), 1392, <https://doi.org/10.3390/w10101392>, 2018.

686 Matsuura, K., and Willmott C. J.: Terrestrial precipitation: 1900–2008 gridded monthly time series
687 (version 2.01), Center for Climatic Research Department of Geography Center for Climatic
688 Research, University of Delaware,
689 http://climate.geog.udel.edu/~climate/html_pages/Global2_Ts_2009/README.global_p_ts_2009.html, 2009.

691 Mitchell, T. D., and Jones, P. D.: An improved method of constructing a database of monthly climate
692 observations and associated high-resolution grids, *Int. J. Climatol.*, 25, 693-712,
693 <https://doi.org/10.1002/joc.1181>, 2005.

694 Rajeevan, M., and Bhate, J.: A high resolution daily gridded rainfall dataset (1971–2005) for mesoscale
695 meteorological studies, *Curr. Sci.*, 96, 558-562, <https://www.jstor.org/stable/24105470>, 2009.

696 Rozante, J. R., Moreira, D. S., Goncalves, L.G., and Vila, D. A.: Combining TRMM and surface
697 observations of precipitation: technique and validation over South America, *Wea. Forecasting*, 25,
698 885-894, <https://doi.org/10.1175/2010WAF2222325.1>, 2010.

699 Schneider, U., Fuchs, T., Meyer-Christoffer, A., and Rudolf, B.: Global precipitation analysis

700 products of the GPCC. Global Precipitation Climatology Centre, DWD, 13 pp., 2008

701 Schneider, U., Becker, A., Finger, P., Meyer-Christoffer, A., Ziese, M., and Rudolf, B.: GPCC's new land
702 surface precipitation climatology based on quality-controlled in situ data and its role in
703 quantifying the global water cycle, *Theor. Appl. Climatol.*, 115, 15-40,
704 <https://doi.org/10.1007/s00704-013-0860-x>, 2014.

705 Schneider, U., P. Finger, A. Meyer-Christoffer, M. Ziese, A. Becker: Global Precipitation Analysis
706 Products of the GPCC. GPCC Internet Publication, DWD, 17 pp., 2018

707 Shen, Y., Feng, M. N. Zhang, H. Z. and Gao, X.: Interpolation methods of China daily precipitation data
708 [in Chinese], *J. Appl. Meteorol. Sci.*, 21, 279–286, <https://doi.org/10.11898/1001-7313.20100303>,
709 2010.

710 Shen, Y., Zhao, P., Pan, Y., and Yu, J.: A high spatiotemporal gauge-satellite merged precipitation analysis
711 over China, *J. Geophys. Res. Atmos.*, 119, <https://doi.org/10.1002/2013JD020686>, 2014.

712 Sorooshian, S., Hsu, K.-L., Gao, X., Gupta, H. V., Imam, B., and Braithwaite, D.: Evaluation of
713 PERSIANN System Satellite-Based Estimates of Tropical Rainfall, *Bull. Amer. Meteorol. Soc.*,
714 81, 2035-2046, [https://doi.org/10.1175/1520-0477\(2000\)081<2035:EOPSSE>2.3.CO;2](https://doi.org/10.1175/1520-0477(2000)081<2035:EOPSSE>2.3.CO;2), 2000.

715 Sunilkumar, K., Yatagai, A., and Masuda, M.: Preliminary evaluation of GPM-IMERG rainfall estimates
716 over three distinct climate zones with APHRODITE. *Earth Space Sci.*, 6, 1321– 1335.
717 <https://doi.org/10.1029/2018EA000503>, 2019.

718 Tang, G., Ma, Y., Long, D., Zhong, L., and Hong, Y.: Evaluation of GPM Day-1 IMERG and TMPA

719 Version-7 legacy products over Mainland China at multiple spatiotemporal scales, *J. Hydrol.*, 533,
720 152-167, <https://doi.org/10.1016/j.jhydrol.2015.12.008>, 2016.

721 Tang, G., Clark, M. P., Papalexiou, S. M., Ma, Z., and Hong, Y.: Have satellite precipitation products
722 improved over last two decades? A comprehensive comparison of GPM IMERG with nine satellite
723 and reanalysis datasets, *Remote Sens. Environ.*, 240, 111697,
724 <https://doi.org/10.1016/j.rse.2020.111697>, 2020.

725 Xie, P., and Xiong, A.: A conceptual model for constructing high-resolution gauge-satellite merged
726 precipitation analyses, *J. Geophys. Res. Atmos.*, 116, <https://doi.org/10.1029/2011JD016118>,
727 2011.

728 Xu, J., Ma, Z., Tang, G., Ji, Q., Min, X., Wan, W., and Shi, Z.: Quantitative Evaluations and Error Source
729 Analysis of Fengyun-2-Based and GPM-Based Precipitation Products over Mainland China in
730 Summer, 2018, *Remote Sens.*, 11, <https://doi.org/10.3390/rs11242992>, 2019.

731 Yatagai, A., Xie, P., and Kitoh, A.: Utilization of a New Gauge-based Daily Precipitation Dataset over
732 Monsoon Asia for Validation of the Daily Precipitation Climatology Simulated by the MRI/JMA
733 20-km-mesh AGCM, *SOLA*, 1, 193-196, <https://doi.org/10.2151/sola.2005-050>, 2005.

734 Yatagai, A., Kamiguchi, K., Arakawa, O., Hamada, A., Yasutomi, N., and Kitoh, A.: APHRODITE:
735 Constructing a Long-Term Daily Gridded Precipitation Dataset for Asia Based on a Dense Network
736 of Rain Gauges, *Bull. Amer. Meteorol. Soc.*, 93, 1401-1415, [https://doi.org/10.1175/BAMS-D-11-](https://doi.org/10.1175/BAMS-D-11-00122.1)
737 00122.1, 2012.

738 Yong, B., Ren, L.-L., Hong, Y., Wang, J.-H., Gourley, J. J., Jiang, S.-H., Chen, X., and Wang, W.:
739 Hydrologic evaluation of Multisatellite Precipitation Analysis standard precipitation products in
740 basins beyond its inclined latitude band: A case study in Laohahe basin, China, *Water Resour. Res.*,
741 46, <https://doi.org/10.1029/2009WR008965>, 2010.

742

743

744

745 **Appendix A: Acronyms with definitions used in this study.**

AIMERG	Asian precipitation dataset by calibrating GPM IMERG at daily scale using APHRODITE
APHRODITE	Asian Precipitation Highly Resolved Observational Data Integration Towards Evaluation of Water Resources
ATBD	Algorithm Theoretical Basis Document
BIAS	Relative Bias
CC	Correlation Coefficient
CHIRPS	Climate Hazards group Infrared Precipitation with Stations
CLIMAT	Monthly Climatological Data
CMA	Chinese Meteorological Administration
CMORPH	Climate Prediction Center (CPC) MORPHing technique
CPC	Climate Prediction Center
CSI	Critical Success Index
DSTDCA	Daily Spatio-Temporal Disaggregation Calibration Algorithm
DWD	Deutscher Wetterdienst
ERA5	Fifth generation of ECMWF atmospheric reanalyses of the global climate
ERA-Interim	ECMWF ReAnalysis Interim
FAR	False Alarm Ratio
GEWEX	Global Energy and Water Exchange
GPCC	Global Precipitation Climatology Centre

GPM	Global Precipitation Measurement
GSMaP	Gauge-adjusted Global Satellite Mapping of Precipitation V7
GTS	Global Telecommunications System
IMERG	Integrated Multi-satellitE Retrievals for GPM
IR	Infrared
MAE	Mean Absolute Error
MERRA2	The Modern-Era Retrospective Analysis for Research and Applications, Version 2
MW	Microwave
NHMs	National hydrological and meteorological services
NMIC	National Meteorological Information Center
OI	Optimal Interpolation
PDF	Probability Density Function
PERSIANN	Precipitation Estimation from Remotely Sensed Information using Artificial Neural Networks
PERSIANN- CCS	Precipitation Estimation from Remotely Sensed Information using Artificial Neural Networks-Cloud Classification System
PERSIANN- CDR	PERSIANN-Climate Data Record
PMW	Passive Microwave
POD	Probability of Detection

QC	Quality Control
RMSD	Root Mean Square Deviation
RMSE	Root Mean Square Error
SG	Satellite-Gauge
SM2RAIN	Soil Moisture to RAIN based on ESA Climate Change Initiative (CCI)
SYNOP	Synoptic Weather Report
TMPA	TRMM Multi-satellite Precipitation Analysis
TRMM 3B42	Tropical Rainfall Measuring Mission Multi-satellite Precipitation Analysis 3B42 V7